Executioner caspase is proximal to Fasciclin 3 which facilitates non-lethal activation in *Drosophila* olfactory receptor neurons

Authors

Masaya Muramoto[a,1], Nozomi Hanawa[a,1], Misako Okumura[b,c], Takahiro Chihara[b,c], Masayuki Miura[a,2], and Natsuki Shinoda[a,2]

Affiliations & Footnotes

[a] Department of Genetics, Graduate School of Pharmaceutical Sciences, University of Tokyo, 7-3-1 Hongo, Bunkyo-ku, Tokyo 113-0033, Japan

[b] Program of Biomedical Science, Graduate School of Integrated Sciences for Life, Hiroshima University, Higashi-Hiroshima, Hiroshima 739-8526, Japan

[c] Program of Basic Biology, Graduate School of Integrated Sciences for Life, Hiroshima University, Higashi-Hiroshima, Hiroshima 739-8526, Japan

[1] Equal contributions

[2] Corresponding authors

Corresponding Authors

Masayuki Miura: Department of Genetics, Graduate School of Pharmaceutical Sciences, University of Tokyo, 7-3-1 Hongo, Bunkyo-ku, Tokyo 113-0033, Japan. Telephone: +81-3-5841-4860. E-mail: miura@mol.f.u-tokyo.ac.jp

Natsuki Shinoda: Department of Genetics, Graduate School of Pharmaceutical Sciences, University of Tokyo 7-3-1 Hongo, Bunkyo-ku, Tokyo 113-0033, Japan. Telephone: +81-3-5841-4867. E-mail: f-shinoda.natsuki@g.ecc.u-tokyo.ac.jp

Abstract

The nervous system undergoes functional modification independent on cell turn over. Caspase participates in reversible neuronal modulation via non-lethal activation. However, the mechanism that enables non-lethal activation remains unclear. Here, we analyzed proximal proteins of *Drosophila* executioner caspase in the adult brain using TurboID. We discovered that executioner caspase Drice is, as an inactive proform, proximal to cell membrane proteins, including a specific splicing isoform of cell adhesion molecule Fasciclin 3 (Fas3), Fas3G. To investigate whether sequestration of executioner caspase to plasma membrane of axons is the mechanism for non-lethal activation, we developed a Gal4-Manipulated Area-Specific CaspaseTracker/CasExpress system for sensitive monitoring of caspase activity near plasma membrane. We demonstrated that *Fas3G*-overexpression promotes caspase activation in olfactory receptor neurons without killing them, by inducing expression of initiator caspase Dronc, which also comes close to Fas3G. Physiologically, *Fas3G*-overexpression facilitated non-lethal activation suppresses innate olfactory attraction behavior. Our findings suggest that subcellularly-restricted caspase activation, defined by caspase proximal proteins, is the mechanism for non-lethal activation, opening the methodological development of reversible modification of neuronal function via regulating caspase proximal proteins.

44 **Introduction**

45 During and even after development, the nervous system undergoes functional modification
46 usually not depending on cell turn over. Caspase, best known as a cysteine aspartic acid protease
47 involved in cell death, participates neuronal functional modulation through non-lethal
48 activation (Mukherjee and Williams, 2017). In zebrafish embryo, non-lethal caspase activity
49 promotes axon arbor dynamics in retinal ganglion cells (Campbell and Okamoto, 2013). In
50 *Drosophila*, caspase activation promotes engulfment of pruned dendrites during metamorphosis
51 (Williams et al., 2006). Furthermore, non-lethal caspase activity promotes the maturation of
52 olfactory sensory neurons during development in mice (Ohsawa et al., 2010). In the mature
53 nervous system, non-lethal caspase activity induces long-term depression by AKT cleavage in
54 mice (Li et al., 2010). These processes are termed caspase-dependent non-lethal cellular
55 processes (CDPs)(Aram et al., 2017). While a growing number of CDPs have been identified
56 (Nakajima and Kuranaga, 2017), relatively less is known about its regulatory mechanisms that
57 enable specific non-lethal functions without causing cell death especially in nervous systems
58 (Mukherjee and Williams, 2017). One potential mechanism is the restriction of the extent and
59 spread of activated caspases (Mukherjee and Williams, 2017), yet experimental evidence is
60 limited.

61 Proteins that interact with initiator caspases are among the key regulators of CDPs.
62 Tango7, the *Drosophila* translation initiation factor eIF3 subunit m, acts as an adapter and
63 regulates the localization of the initiator caspase Dronc. During sperm individualization,
64 Tango7 directs Dronc to the individualization complex (D'Brot et al., 2013). In salivary glands,
65 Tango7 directs Dronc to the plasma membrane (Kang et al., 2017). In both cases, caspase
66 activity promotes cellular remodeling without inducing cell death (D'Brot et al., 2013; Kang et
67 al., 2017). CRINKLED, a *Drosophila* unconventional myosin, functions as an adaptor of Dronc
68 and facilitates the cleavage of Shaggy46 (Orme et al., 2016). Shaggy46, activated by caspase-

69 mediated cleavage, suppresses the emergence of ectopic sensory organ precursors (Kanuka et
70 al., 2005). During apoptosis-induced proliferation (AiP), Myo1D, another *Drosophila*
71 unconventional myosin, facilitates Dronc translocation to the basal side of the plasma
72 membrane of imaginal discs to promote AiP (Amcheslavsky et al., 2018). Thus, initiator
73 caspase-interacting proteins regulate caspase activity in CDPs. However, given the importance
74 of executioner caspases, which are activated by the initiator caspase to cleave a broad range of
75 substrates and are essential for apoptosis (Julien and Wells, 2017; Kumar, 2007), little is known
76 about the subcellular compartmentalization and interacting proteins of those involved in CDPs.
77 This lack of understanding is partly due to the absence of protein-protein interaction domains
78 (e.g., DED and CARD) in the N-terminus of executioner caspases (Kumar et al., 2022).

79 To understand the molecular mechanism regulating caspase activity involved in CDPs,
80 we focused on the proximal proteins of executioner caspases using TurboID, a proximity
81 labeling technique that analyzes protein proximity *in vivo* (Branon et al., 2018; Qin et al., 2021).
82 We previously established C-terminal TurboID knocked-in caspase fly lines for Dronc
83 (initiator), Drice (executioner), and Dcp-1 (executioner)(Shinoda et al., 2019). Importantly, we
84 have demonstrated that one of the preferred substrates of Drice, BubR1, is proximal to Drice *in*
85 *vivo* (Shinoda et al., 2023), suggesting that substrate preference is exploited by protein
86 proximity. Therefore, the proximity of executioner caspases to proteins is emerging as a means
87 of regulating specific non-lethal functions.

88 To investigate the regulatory mechanisms of non-lethal function of caspase in the
89 nervous system, we conducted comprehensive analysis of proximal proteins of executioner
90 caspase Drice. We discovered that Drice is, as an inactive proform, primarily proximal to cell
91 membrane proteins, including cell adhesion molecule Fasciclin 3 (Fas3). Notably, Drice is
92 proximal to the specific alternative splicing isoforms of Fas3, Fas3G. To ascertain whether
93 Fas3G modulates caspase activity, we developed a Gal4-Manipulated Area Specific

94 CaspaseTracker/CasExpress (MASCaT) system, which permits the monitoring of caspase
95 activity near plasma membrane with high sensitivity and simultaneous genetic manipulation in
96 the cells of interest. Using MASCaT, we demonstrated that *Fas3G* overexpression enhances
97 caspase activation without killing olfactory receptor neurons through the induction of the
98 expression of initiator caspase Dronc, which also comes proximal to Fas3G. Subsequently, we
99 showed that *Fas3G* overexpression-facilitated non-lethal caspase activation in olfactory
100 receptor neurons suppresses innate olfactory attraction behavior. Collectively, our findings
101 suggest that caspase activation is subcellularly restricted, the platform of which is defined by
102 caspase proximal proteins, for non-lethal functions. In contrast to lethal activation, suppressing
103 neuronal activity with non-lethal caspase activation is reversible. By regulating caspase
104 proximal proteins, reversible modification of neuronal functional by non-lethal caspase
105 activation will be achieved.
106

107 **Results**

108 ***Drice is the major executioner caspase expressed in the adult brains***

109 Apoptotic stimuli activate initiator caspases that trigger a proteolytic cascade, leading to the
110 activation of executioner caspases and culminating in apoptosis (Green, 2019). In *Drosophila*,
111 the caspase-mediated apoptotic signaling pathway is highly conserved (Figure 1A)(Nakajima
112 and Kuranaga, 2017). The activity of executioner caspases, specifically Drice and Dcp-1, is
113 regulated by apoptotic signaling pathways, including the initiator caspase Dronc (Figure 1A).
114 To investigate the expression patterns of *Drosophila* caspases, we employed
115 *Caspase::V5::TurboID* knocked-in fly lines (Shinoda et al., 2019). We found low levels of
116 expression of the initiator caspase Dronc in adult heads (Figure 1B). Conversely, we observed
117 high expression of the executioner caspase Drice, whereas Dcp-1 was expressed at lower levels
118 in adult heads (Figure 1B). The proximal proteins of each caspase were labeled with TurboID
119 in adult heads by administration of 100 μM biotin (Figure 1B). Furthermore, we investigated
120 the expression patterns of caspases using histochemical analysis by examining streptavidin
121 (SA) signal. Consistent with the western blotting findings, Drice showed higher expression
122 levels than Dronc and Dcp-1, which were expressed at lower levels (Figure 1C). We found that
123 Drice was expressed in distinct regions, including the mushroom bodies (MBs), suboesophageal
124 ganglions (SGs), optic lobes (OLs), and antennal lobes (ALs), which showed the highest levels
125 of expression (Figure 1C). The *Drosophila* ALs comprise synaptic contacts between the axons
126 of olfactory receptor neurons (ORNs), the dendrites of projection neurons (PNs), and local
127 interneuron (LNs) processes. Neuron-type-specific Gal4s were used to knockdown *Drice* and
128 the expression patterns were subsequently examined. We found that Drice was expressed
129 predominantly in ORNs in the AL (Figure 1D). These results showcase that Drice is not
130 expressed in the entire brain, but rather in a specific subset of neurons in the adult brains.
131 Comparisons of the expression patterns of Drice were consistent across both males and females

132 (Figure 1–figure supplement 1A), indicating an absence of sex-based differences, which
133 justifies the use of males for functional simplicity in this study.
134
135 ***Drice is proximal to cell membrane proteins rather than cytosolic proteins in the adult brains***
136 To comprehensively identify proximal proteins of Drice, we employed a proximity labeling
137 approach. Specifically, we used *Drice::V5::TurboID* knocked-in flies fed 100 μM biotin. We
138 confirmed biotinylation of Drice proximal proteins in the adult brains (Figure 1E). After
139 purifying the biotinylated proteins using NeutrAvidin magnetic beads, we performed LC-
140 MS/MS analysis of the samples (Figure 1F). We identified 643 proteins (Figure 1G, Table S1),
141 of which 158 were highly specific to *Drice::V5::TurboID* flies compared to wild-type flies
142 (*Drice::V5::TurboID*/w^{1118} > 10; Figure 1G, Table S1). Gene ontology analysis revealed that
143 Drice proximal proteins were enriched in the plasma membrane, synaptic vesicles, postsynaptic
144 membranes, and adherens junctions (Figure 1H, Table S2). This finding suggests that Drice is
145 localized primarily in cell membrane compartments rather than in the cytoplasm of the adult
146 brain. Additionally, because the SA signal of *Drice::V5::TurboID* is mainly observed in the
147 AL where the axons of ORNs project (Figure 1C), the enrichment of cell membrane proteins in
148 the proximal proteins of Drice is reasonable.
149
150 ***A specific splicing isoform of Fasciclin 3 is in proximity to Drice***
151 During our analysis of proteins proximal to Drice, we discovered that the expression patterns
152 of Fasciclin 3 (Fas3) in the adult brain closely resembled those of Drice, especially within the
153 OLs, SGs, and ALs (Figure 2A, B). Thus, we focused on Fas3 (Chiba et al., 1995), a
154 transmembrane protein containing immunoglobulin-like domains that regulates synaptic target
155 recognition and axon fasciculation (Kose et al., 1997). *Fas3* is encoded by seven splicing
156 isoforms, resulting in the production of five protein isoforms that share extracellular domains

157 but differ in intracellular domains with low-complexity sequences (Figure 2C, D). Only one
158 specific protein isoform, Fas3 isoform G (Fas3G), was identified in the LC-MS/MS analysis as
159 a Drice-proximal protein in the adult brain (Figure 1G, Table S1). Using AlphaFold2-Multimer
160 (Evans et al., 2021; Mirdita et al., 2022), Drice was predicted to interact with Fas3A (ipTM =
161 0.456) and Fas3G (ipTM = 0.372) rather than Fas3C (ipTM = 0.298), Fas3D/E (ipTM = 0.220)
162 and Fas3B/F (ipTM = 0.207). Among Fas3 isoforms, only Fas3G is predicted to interact with
163 Drice with 2 intracellular regions (Figure 2–figure supplement 1A). To validate this result, we
164 generated an antibody specific to Fas3G (Figure 2C, E). We confirmed that only the Fas3G was
165 labeled with Drice::V5::TurboID and purified using NeutrAvidin magnetic beads as detected
166 using western blotting (Figure 2F). To further confirm the isoform specificity to Drice
167 proximity, we overexpressed 3xFLAG-tagged *Fas3 isoforms A*, *B/F*, *C*, *D/E*, and *G* in olfactory
168 receptor neurons using *Pebbled-Gal4* in a *Drice::V5::TurboID* knocked-in background. After
169 proximity labeling with TurboID, followed by NeutrAvidin purification, we found that the
170 Fas3G was highly enriched compared to the other isoforms (Figure 2G). These findings
171 suggested that Drice is proximal to a specific isoform of Fas3 in olfactory receptor neurons,
172 regardless of its protein expression level. We also investigated whether Drice and Fas3G
173 statically interact by co-immunoprecipitation. Although Fas3G was labelled by
174 Drice::V5::TurboID, indicating its proximity to Drice within the ORNs of adult brains, Drice
175 did not co-immunoprecipitate with Fas3G (Figure 2–figure supplement 2A). This result
176 suggests that while Drice and Fas3G are proximate, their interaction is not static, highlighting
177 the utility of proximity labeling as a superior technique to conventional co-immunoprecipitation
178 for identifying proteins that are spatially close.
179
180 ***Fasciclin 3s are not substrates of caspase***

181 It is often observed that proteins in close proximity to caspases are their preferred substrates
182 (Shinoda et al., 2023). To investigate this, we examined whether any of the Fas3 isoforms are
183 substrates for caspase by expressing all isoforms in *Drosophila* S2 cells. However, we found
184 that none of the Fas3 isoforms were cleaved by caspase following the induction of apoptosis
185 (Figure 2–figure supplement 2B). Therefore, Fas3s are not substrates of caspase.
186
187 ***MASCaT: a cell type-specific highly sensitive non-lethal caspase activity reporter***
188 We investigated whether Fas3G regulates caspase activity in lethal or non-lethal processes.
189 CaspaseTracker/CasExpress is a highly sensitive reporter of non-lethal caspase activity that
190 uses caspase-activatable Gal4 tethered to the membrane by mCD8 (Ding et al., 2016; Tang et
191 al., 2015). However, reliance on Gal4 to report their activity presents a challenge in reconciling
192 Gal4/UAS-dependent gene manipulations. To overcome this limitation, we created a new
193 reporter to capture non-lethal caspase activation independent of caspase-activatable Gal4. We
194 replaced the caspase-activatable Gal4 with the caspase-activatable QF2 (*mCD8::DQVD::QF2*),
195 where DQVD is a caspase cleavage sequence, and first expressed directly downstream of *UAS*
196 sequence (Figure 3–figure supplement 1A). However, the caspase-activatable QF2 induced
197 mNeonGreen expression under *QUAS* sequence even either with a pan-caspase inhibitor,
198 zVAD-fmk, or an uncleavable DQVA mutant probe (*mCD8::DQVA::QF2*, insensitive to
199 caspase-mediated cleavage which serves as a negative control) (Figure 3–figure supplement
200 1B), potentially because the Gal4/UAS binary system expressed excessive
201 mCD8::DQVD/A::QF2 probes that results in caspase activation-independent induction of
202 QF2/QUAS system. Thus, to reduce the amount of probes expression, we generated *Ubi-FRT-*
203 *STOP-FRT-mCD8::DQVD::QF2*, simultaneously expressing *Flippase* (*FLP*) under *UAS* to
204 restrict reporter expression to the cells of interest (Figure 3A). *Drosophila* S2 cells undergo
205 weak caspase activation only by transfection (Shinoda et al., 2023). Taking advantage of that,

206 this system reports caspase activity through the caspase-activatable QF2/QUAS system,
207 expressing mNeonGreen, which is not detected by caspase-non-activatable QF2 (Figure 3B).
208 We named this novel reporter a Gal4-Manipulated Area Specific CaspaseTracker/CasExpress
209 (MASCaT; Figure 3A). Using MASCaT, we detected non-lethal caspase activity, specifically
210 in the neurons of adult brains, using *ELAV-Gal4* (Figure 3C). Caspase activity was prominent
211 in OLs (Figure 3C), which is consistent with the previously reported activation pattern of
212 caspase detected by CaspaseTracker/CasExpress (Ding et al., 2016; Tang et al., 2015).
213 Previously, we reported that a specific subset of ORNs, including Or42b, undergoes age-
214 associated caspase activation (Chihara et al., 2014). Consistent with this finding, we detected
215 age-dependent caspase activation in the AL (Figure 3C). Therefore, our newly established
216 reporter, MASCaT, enables the highly sensitive detection of caspase activity near the plasma
217 membrane in cells of interest reconciling with Gal4/UAS-dependent gene manipulations.
218
219 ***Fas3G overexpression activates caspase in a non-lethal manner***
220 To investigate the regulatory role of Fas3 in caspase activity *in vivo*, we used Or42b neurons as
221 a model, which have previously been shown to undergo age-dependent caspase activation
222 (Chihara et al., 2014). Initially, we evaluated the effects of *Dronc* overexpression on apoptosis
223 by quantifying cell body numbers in the antenna in young flies. Dronc induced cell loss while
224 catalytically inactive Dronc ($Dronc^{CG}$) did not, suggesting that Dronc induce apoptosis in a
225 catalytic-dependent manner (Figure 4A, B). We then evaluated the effects of the overexpression
226 of the executioner caspases *Dcp-1* and *Drice*. Interestingly, although Dcp-1 induced complete
227 cell loss, Drice did not (Figure 4A, B), suggesting that Drice requires an initiator caspase for
228 activation, whereas Dcp-1 does not. These results indicate that Or42b neurons are competent in
229 caspase-mediated cell loss and thus serve as a model for evaluating apoptosis. However, the

230 expression of *Fas3G*, even in combination with *Drice*, did not reduce the number of cells,
231 implying that *Fas3G* overexpression did not induce apoptosis (Figure 4C, D).

232 Subsequently, we assessed the regulation of non-lethal caspase activity by Fas3G *in*
233 *vivo*. We first confirmed that MASCaT probes were distributed in the axons of ORNs (Figure
234 4E). Using MASCaT, we observed weak non-lethal caspase activation even in the control group
235 at a young age (Figure 4F, G). The expression of *Fas3G* significantly promoted caspase
236 activation (Figure 4F, G), indicating that Fas3G regulates non-lethal caspase activation.
237 Moreover, the simultaneous expression of *Drice* and *Fas3G* significantly enhanced caspase
238 activation (Figure 4F, G), signifying the promoting effect of their proximity. Moreover, the
239 concurrent expression of Diap-1, an E3 ligase known to inhibit caspase activation (Ditzel et al.,
240 2008; Hay et al., 1995; Lee et al., 2011), mitigated the caspase activation induced by *Fas3G*
241 overexpression (Figure 4H, I). This indicates that *Fas3G* overexpression-facilitated non-lethal
242 caspase activation is dependent on the core apoptotic machinery. To test whether endogenous
243 Fas3G regulates caspase activation, we generated *Fas3G*-specific *shRNA* expressing strain
244 (Figure 4–figure supplement 1A, B). Knockdown of *Fas3* or *Fas3G* in Or42b neurons didn't
245 suppress the inherent, weak caspase activation (Figure 4–figure supplement 1C, D). In
246 agreement with this, Drice's presence in the axon of ORNs with Fas3G was observed, yet its
247 presence was not strictly contingent on Fas3 or Fas3G (Figure 4–figure supplement 1E). Given
248 the numerous other membrane proteins in proximity to Drice (Figure 1G, H and Table S1), it is
249 probable that additional proteins may be responsible for recruiting Drice to the axon. These
250 findings collectively imply that while Fas3G is not essential for mild endogenous caspase
251 activation, overexpression of *Fas3G* does enhance non-lethal caspase activation in ORNs, thus
252 providing a valuable model for exploring the molecular processes that facilitate caspase
253 activation without leading to cell death.
254

255 ***Fas3G is proximal to Dronc which is required for non-lethal caspase activation***

256 Next, we investigated the underlying mechanism that enhances non-lethal activation facilitated
257 by *Fas3G* overexpression. Executioner caspases, Drice and Dcp-1, are activated by initiator
258 caspases, Dronc (Figure 1A). We precisely analyzed expression pattern of Dronc in adult brains
259 and found that while its expression was low in control, overexpression of *Fas3G* in ORNs
260 markedly increased Dronc levels in those neurons (Figure 5A). Moreover, akin to Drice, Dronc
261 was also found in close proximity to the overexpressed Fas3G, but not to the overexpressed
262 Fas3C in ORNs (Figure 5B). Consequently, we examined whether Dronc is required for the
263 non-lethal caspase activation enhanced by *Fas3G* overexpression. Employing MASCaT, we
264 discovered that both knockdown of *Dronc* and the expression of the *dominant-negative form of*
265 *Dronc* hindered the non-lethal caspase activation facilitated by *Fas3G* overexpression (Figure
266 5C, D), indicating a dependence on initiator caspase activity. Importantly, the genetic
267 suppression of Dronc activity did not alter the proximity between Drice and Fas3G (Figure 5E),
268 suggesting that the inactive Drice proform is primarily proximal to Fas3G. Solo overexpression
269 of *Dronc* led to cell death in Or42b neurons (Figure 4A, B), whereas *Fas3G* overexpression
270 elevated Dronc expression without causing cell death (Figure 4C, D, Figure 5A). Collectively,
271 these findings imply that the non-lethal caspase activation driven by *Fas3G* overexpression is
272 orchestrated by an increase in Dronc induced by Fas3G, bringing Dronc in close vicinity to
273 Fas3G and thus enabling caspase activation near the plasma membrane (Figure 5F).

274

275 ***Non-lethal caspase activation regulates innate attraction behavior***

276 Finally, we examined the function of *Fas3G* overexpression-facilitated non-lethal caspase
277 activation. Apple cider vinegar (ACV) excites six glomeruli in the AL, including DM1, which
278 is innervated by the axons of Or42b neurons (Semmelhack and Wang, 2009). We have
279 previously reported that Or42b neurons undergo aging-dependent caspase activation and cell

280 death, which reduces neuronal activity and attraction behavior in response to ACV (Chihara et
281 al., 2014). Inhibition of caspase activity in aged flies restores attraction behavior but does not
282 affect that of young flies (Chihara et al., 2014). Using a two choice preference assay with ACV
283 (Figure 6A), we found that the overexpression of *Fas3G*, which activates caspases, did not
284 impair attraction behavior in young flies (Figure 6B, C). In contrast, simultaneous inhibition of
285 *Fas3G* overexpression-facilitated non-lethal caspase activation promoted attraction to ACV
286 (Figure 6B, C). Overall, these results suggest that *Fas3G* overexpression-facilitated non-lethal
287 caspase activation suppresses innate attractive behavior even without killing the cells.
288

289 **Discussion**

290 ***Proximal proteins of executioner caspases regulate non-lethal caspase activity***

291 It is important to identify the proximal proteins of executioner caspases, which cleave a wide
292 range of substrates and are essential for apoptosis (Julien and Wells, 2017; Kumar, 2007), as
293 proximity often dictates substrate specificity (Shinoda et al., 2023). In humans, caspase-3 and
294 caspase-7 have been shown to share but also have discrete substrate preferences (Walsh et al.,
295 2008). Caspase-7 leverages an exosite to facilitate interaction with RNA and enhance the
296 proteolysis of RNA-binding proteins (Boucher et al., 2012; Desroches and Denault, 2019). Thus,
297 protein proximity can be used to precisely regulate specific cellular functions by selectively
298 cleaving a limited pool of substrates in non-lethal scenarios compared with lethal cleavages
299 where all the substrates are potentially cleaved during apoptosis. We showed that executioner
300 caspases, before activation as proforms, are exclusively sequestered in specific subcellular
301 domains, including the plasma membrane. We found that *Fas3G* overexpression facilitates non-
302 lethal activation, underscoring the importance of protein proximity not only in substrate
303 cleavage, but also in localizing non-lethal activation to the vicinity of plasma membrane (Figure
304 5F). Our results suggest that subcellularly restricted caspase activation mediated by caspase
305 proximal proteins is one of the potential mechanisms regulating caspase activation without
306 inducing cell death.

307

308 ***MASCaT as a highly sensitive reporter for identifying non-lethal caspase regulators***

309 Various caspase activity reporters have been developed, including SCAT3, a FRET-based
310 reporter with superior temporal resolution (Takemoto et al., 2003), CaspaseTracker/CasExpress,
311 Caspase-activatable Gal4-based reporters with superior sensitivity (Ding et al., 2016; Tang et
312 al., 2015). However, to date, no reporter has been developed that is sensitive enough to identify
313 non-lethal regulators of caspases in cells of interest. In this study, we developed a novel caspase

314 reporter, MASCaT, that can detect non-lethal caspase activation with high sensitivity in a cell
315 type-specific manner following gene manipulation. Using MASCaT, we identified previously
316 overlooked regulators of non-lethal activation of caspases in a cell type-specific manner.
317 Proximal proteins of executioner caspases are potential non-lethal regulators, and combining
318 TurboID-mediated identification of these proteins will pave the way for identifying non-lethal
319 components and broaden our understanding of the molecular mechanism of non-lethal caspase
320 activation.
321
322 ***Non-lethal caspase activation regulates neuronal activity and behaviors***
323 We previously reported that age-dependent caspase activation reduces neuronal activity and
324 innate attraction behavior (Chihara et al., 2014). Here, we found that, while *Fas3G*
325 overexpression did not impair attraction behavior by itself, caspase activation upon *Fas3G*
326 overexpression suppressed attraction behavior toward ACV (Figure 6A, B). In mice, L1CAM,
327 an immunoglobulin-like cell adhesion molecule, facilitates neuronal excitability by regulating
328 the voltage-gated Na+ channels (Valente et al., 2016). Thus, we hypothesize that non-lethal
329 caspase activation antagonizes the neuronal excitability promoted by Fas3G. In neurons,
330 caspases have diverse non-lethal functions, including axon degeneration and macro- and micro-
331 pruning, to regulate synaptic plasticity (Dehkordi et al., 2022; Mukherjee and Williams, 2017).
332 In presynaptic terminals, it has been recently reported that Caspase-3 modulates synaptic
333 vesicle pools via autophagy (Gu et al., 2021). Thus, it is possible that non-lethal activation
334 regulates synaptic pools and neuronal activity in a reversible manner without killing the cells.
335 Analyzing the functions mediated by Drice and Fas3G proximity, including the identification
336 of specific substrates, will pave the way for identifying diverse CDPs and understanding their
337 molecular mechanisms.

338 While suppressing innate attraction behavior does not seem beneficial by itself, it
339 should be a great advantage in decision-making. To survive, flies must constantly make
340 appropriate behavioral decisions (e.g., feeding versus mating) depending on their physiological
341 conditions. In males, a subset of neurons regulated by tyramine controls feeding versus mating
342 behaviors (Cheriyamkunnel et al., 2021). In regard of that, it is important to adequately promote
343 or suppress neuronal activity, which controls behaviors of the organisms, by precisely
344 controlling caspase activation in a subcellularly restricted manner in neurons. Compared with
345 lethal activation which irreversibly removed the neurons of interest, suppressing neuronal
346 activity with non-lethal reversible caspase activation is beneficial for decision makings
347 depending on their varying physiological conditions. As regulating caspase proximal proteins
348 enables non-lethal activation which is not achieved by directly manipulating caspase expression,
349 our results open the possibility of the methodological development for reversible manipulation
350 of neuronal activity via non-lethal caspase activity.
351
352 ***Proximal proteins of executioner caspases define the site of caspase activation "hotspot"***
353 Although the core apoptotic machinery has been well characterized during the last 30 years
354 (Nakajima and Kuranaga, 2017), the precise regulation of CDPs, remains incompletely
355 elucidated. In this study, we identified *Fas3G* overexpression activates Drice. Mechanistically,
356 we found that *Fas3G* overexpression induced the expression of initiator caspase Dronc, which
357 also comes close to Fas3G, regulating non-lethal caspase activation. Direct overexpression of
358 Dronc alone results in cell death within olfactory receptor neurons (Figure 4A, B). However,
359 when Dronc expression is upregulated due to *Fas3G* overexpression, it does not lead to cell
360 death in ORNs (Figure 4C, D). The exact process by which Dronc expression is increased in
361 response to *Fas3G* overexpression remains to be elucidated. It is known that Dronc can be
362 upregulated via the ecdysone signaling pathway (Dorstyn et al., 1999) and the Hippo signaling

363 pathway (Verghese et al., 2012). Therefore, the overexpression of *Fas3G* might potentially
364 activate Dronc expression through one or both of these signaling pathways. Fas3 is an
365 immunoglobulin-like domain-containing transmembrane protein that regulates axonal
366 fasciculation and neuronal projections (Chiba et al., 1995). NCAM, a mammalian homologue
367 of Fascicilin 2, is an immunoglobulin-like domain-containing cell adhesion molecule. NCAM
368 can physically bind to caspase-8, and depending on NCAM clustering, caspase-8 and -3 are
369 activated and contribute to neurite outgrowth by cleaving its substrate spectrin (Westphal et al.,
370 2010). Thus, it seems likely that cell adhesion molecule-mediated subcellularly restricted
371 caspase activation is conserved among species. Indeed, caspase-9/Apaf-1-dependent caspase-3
372 activation, without resulting in cell death, has also been observed in the axon of olfactory
373 sensory neurons during mouse development (Ohsawa et al., 2010).

374 While the restriction of the extent and spread of activated caspases is proposed as one
375 of the potential molecular mechanisms for non-lethal activation (Mukherjee and Williams,
376 2017), experimental evidences are limited. A critical insight from our research is that the
377 executioner caspase is pre-compartmentalized in proximity to a specific set of proteins prior to
378 activation, poised for the initiator caspase to approach. Consequently, the "hotspot" for non-
379 lethal caspase activity appears to be determined by these neighboring proteins of executioner
380 caspases. While the "hotspot" located in the axon of the ORN may exert an inhibitory effect on
381 neuronal activity, it could also play a role in avoiding cell death by localizing caspase activity,
382 especially during development.

383 Recently, a protein interactome analysis in humans showed that tissue-preferentially
384 expressed proteins that interact with known apoptosis regulators participate in apoptosis
385 sensitization (Luck et al., 2020). Given that CDPs are often cell-and tissue type-specific
386 processes, the identification of modulators of context-dependent apoptotic pathways will aid in
387 understanding the precise molecular regulation of CDPs. Importantly, alternative splicing can

388 diversify protein-protein interaction networks. A recent report showed that minor spliceosomes
389 regulate alternative splicing, including Fas3. A specific isoform of Fas3 has distinct functions
390 and cannot be substituted by other isoforms during neuronal development (Li et al., 2020). Our
391 results support the idea that alternative splicing may not only diversify the protein itself, but
392 also its interaction networks to regulate module-dependent activation. Further interactome
393 analysis using TurboID will reveal the regulatory mechanisms of the non-lethal activation of
394 caspases.
395

396 **Methods**

397 ***Fly strains and rearing conditions***

398 We raised the flies in standard *Drosophila* medium at 25°C. For in vivo biotin labeling
399 experiments, flies were raised in standard *Drosophila* medium supplemented with 100 μM (+)-
400 biotin (#132-02635, WAKO). The following fly strains were used in this study: w^{1118},
401 *Drice::V5::TurboID* (Shinoda et al., 2019), *Dcp-1::V5::TurboID* (Shinoda et al., 2019),
402 *Dronc::V5::TurboID* (Shinoda et al., 2019), *Pebbled-Gal4* (BL80570), *LN-Gal4* (BL63325),
403 *GH146-Gal4* (BL30026), *UAS-Drice-RNAi* (V28065),
404 *Fas3::EGFP::FlAsH::StrepII::TEV::3xFLAG* (BL59809), *UASz-Fas3A::3xFLAG* (this study),
405 *UASz-Fas3B::3xFLAG* (this study), *UASz-Fas3C::3xFLAG* (this study), *UASz-*
406 *Fas3D::3xFLAG* (this study), *UASz-Fas3G::3xFLAG* (this study), *Ubi-FRT-STOP-FRT-*
407 *mCD8::DQVD::QF2* (this study), *Ubi-FRT-STOP-FRT-mCD8::DQVA::QF2* (this study),
408 *UAS-FLP* (K107788), *QUAS-tdTomato::3xHA* (BL30005), *ELAV-Gal4* (BL8765), *Or42b-*
409 *Gal4* (BL9971), *UAS-RedStinger* (BL8547), *UASz-myc::mNeonGreen* (this study), *UASz-*
410 *Drice::myc::mNeonGreen* (this study), *UASz-V5::TurboID* (this study), *UASz-*
411 *Drice::V5::TurboID* (this study), *UASz-Drice^{CG}::V5::TurboID* (this study), *UASz-Dcp-*
412 *1::V5::TurboID* (this study), *UASz-Dcp-1^{CG}::V5::TurboID* (this study), *UASz-*
413 *Dronc::V5::TurboID* (this study), *UASz-Dronc^{CG}::V5::TurboID* (this study), *UAS-Diap-*
414 *1::VENUS* (Koto et al., 2009), *UAS-Dronc-RNAi* (Kanuka et al., 2005), *UAS-Dronc^{DN}::EGFP*
415 (Igaki et al., 2002), *UAS-LacZ-RNAi*, *UAS-Fas3-RNAi#1* (V940), *UAS-Fas3-RNAi#2* (V3091),
416 *UAS-Fas3G-RNAi* (this study). BL, Bloomington Drosophila Resource Center; K, Kyoto Stock
417 Center; V, Vienna Drosophila Resource Center.

418

419 ***Detailed genotypes***

420 Figure 1B, C (Left to Right, Top to Bottom)

421 *w^{1118}/Y*

422 *w/Y; Dcp-1::V5::TurboID/+*

423 *w/Y;; Drice::V5::TurboID/+*

424 *w/Y;; Dronc::V5::TurboID/+*

425

426 Figure 1D (Left to Right)

427 *w; UAS-Drice-RNAi/+; Drice::V5::TurboID/+*

428 *w, Pebbled-Gal4/w; UAS-Drice-RNAi/+; Drice::V5::TurboID/+*

429 *w; UAS-Drice-RNAi/GH146-Gal4; Drice::V5::TurboID/+*

430 *w; UAS-Drice-RNAi/+; Drice::V5::TurboID/LN-Gal4*

431

432 Figure 1E (Left to Right)

433 *w^{1118}/Y*

434 *w/Y;; Drice::V5::TurboID/+*

435

436 Figure 1G (Left to Right)

437 *w^{1118}/Y*

438 *w/Y;; Drice::V5::TurboID/+*

439

440 Figure 1–figure supplement 1A (Left to Right, Top to Bottom)

441 *w^{1118}/Y*

442 *w^{1118}*

443 *w/Y;; Drice::V5::TurboID/+*

444 *w/w^{1118};; Drice::V5::TurboID/+*

445

446 Figure 2A (Left to Right)

447 *w^{1118}/Y*

448 *w/Y;; Drice::V5::TurboID/+*

449

450 Figure 2B (Top to Bottom, Left to Right)

451 *w^{1118}/Y*

452 *w/Y;; Drice::V5::TurboID/+*

453 *w/Y; Fas3::EGFP::FlAsH::StrepII::TEV::3xFLAG/+*

454 *w/Y; Fas3:: EGFP::FlAsH::StrepII::TEV::3xFLAG/+; Drice::V5::TurboID/+*

455

456 Figure 2E (Left to Right)

457 *w, Pebbled-Gal4/w or Y*

458 *w, Pebbled-Gal4/w or Y;; UASz-Fas3A::3xFLAG/+*

459 *w, Pebbled-Gal4/w or Y;; UASz-Fas3B::3xFLAG/+*

460 *w, Pebbled-Gal4/w or Y;; UASz-Fas3C::3xFLAG/+*

461 *w, Pebbled-Gal4/w or Y;; UASz-Fas3D::3xFLAG/+*

462 *w, Pebbled-Gal4/w or Y;; UASz-Fas3G::3xFLAG/+*

463

464 Figure 2F (Left to Right)

465 *w^{1118}/Y*

466 *w/Y;; Drice::V5::TurboID/+*

467

468 Figure 2G (Left to Right)

469 *w, Pebbled-Gal4/w or Y;; Drice::V5::TurboID/+*

470 *w, Pebbled-Gal4/w or Y;; Drice::V5::TurboID/UASz-Fas3A::3xFLAG*

471 *w, Pebbled-Gal4/w or Y;; Drice::V5::TurboID/UASz-Fas3B::3xFLAG*

472 *w, Pebbled-Gal4/w or Y;; Drice::V5::TurboID/UASz-Fas3C::3xFLAG*

473 *w, Pebbled-Gal4/w or Y;; Drice::V5::TurboID/UASz-Fas3D::3xFLAG*

474 *w, Pebbled-Gal4/w or Y;; Drice::V5::TurboID/UASz-Fas3G::3xFLAG*

475

476 Figure 2–figure supplement 2A (Left to Right)

477 *w, Pebbled-Gal4/w or Y;; Drice::V5::TurboID/+*

478 *w, Pebbled-Gal4/w or Y;; Drice::V5::TurboID/UASz-Fas3C::3xFLAG*

479 *w, Pebbled-Gal4/w or Y;; Drice::V5::TurboID/UASz-Fas3G::3xFLAG*

480

481 Figure 3C (Top to Bottom)

482 *w/Y; Ubi-FRT-STOP-FRT-mCD8::DQVD::QF2/+; UAS-FLP, QUAS-tdTomato::3xHA/+*

483 *w/Y; Ubi-FRT-STOP-FRT-mCD8::DQVA::QF2/ELAV-Gal4; UAS-FLP, QUAS-*

484 *tdTomato::3xHA/+*

485 *w/Y; Ubi-FRT-STOP-FRT-mCD8::DQVD::QF2/ELAV-Gal4; UAS-FLP, QUAS-*

486 *tdTomato::3xHA/+*

487

488 Figure 4A, B (Top to Bottom, Left to Right)

489 *w/Y; Or42b-Gal4/+; UAS-RedStinger/UASz-V5::TurboID*

490 *w/Y; Or42b-Gal4/+; UAS-RedStinger/UASz-Drice^{CG}::V5::TurboID*

491 *w/Y; Or42b-Gal4/+; UAS-RedStinger/UASz-Drice::V5::TurboID*

492 *w/Y; Or42b-Gal4/+; UAS-RedStinger/UASz-Dcp-1^{CG}::V5::TurboID*

493 *w/Y; Or42b-Gal4/+; UAS-RedStinger/UASz-Dcp-1::V5::TurboID*

494 *w/Y; Or42b-Gal4/+; UAS-RedStinger/UASz-Dronc^{CG}::V5::TurboID*

495 *w/Y; Or42b-Gal4/+; UAS-RedStinger/UASz-Dronc::V5::TurboID*

496

497 Figure 4C, D (Top to Bottom, Left to Right)

498 *w/Y; Or42b-Gal4/UASz-3xFLAG::mNeonGreen; UAS-RedStinger/+*

499 *w/Y; Or42b-Gal4/+; UAS-RedStinger/UASz-Fas3G::3xFLAG*

500 *w/Y; Or42b-Gal4/UASz-Drice::myc::mNeonGreen; UAS-RedStinger/+*

501 *w/Y; Or42b-Gal4/UASz-Drice::myc::mNeonGreen; UAS-RedStinger/UASz-Fas3G::3xFLAG*

502

503 Figure 4E (Top to Bottom)

504 *w/Y; Or42b-Gal4/UASz-3xFLAG::mNeonGreen*

505 *w/Y; Or42b-Gal4, Ubi-FRT-STOP-FRT-mCD8::DQVD::QF2/UASz-3xFLAG::mNeonGreen;*

506 *UAS-FLP, QUAS-tdTomato::3xHA/+*

507

508 Figure 4F, G (Top to Bottom, Left to Right)

509 *w/w or Y; Or42b-Gal4, Ubi-FRT-STOP-FRT-mCD8::DQVD::QF2/UASz-*

510 *3xFLAG::mNeonGreen; UAS-FLP, QUAS-tdTomato::3xHA/+*

511 *w/w or Y; Or42b-Gal4, Ubi-FRT-STOP-FRT-mCD8::DQVD::QF2/+; UAS-FLP, QUAS-*

512 *tdTomato::3xHA/UASz-Fas3G::3xFLAG*

513 *w/w or Y; Or42b-Gal4, Ubi-FRT-STOP-FRT-mCD8::DQVD::QF2/UASz-*

514 *Drice::myc::mNeonGreen; UAS-FLP, QUAS-tdTomato::3xHA/+*

515 *w/w or Y; Or42b-Gal4, Ubi-FRT-STOP-FRT-mCD8::DQVD::QF2/UASz-*

516 *Drice::myc::mNeonGreen; UAS-FLP, QUAS-tdTomato::3xHA/UASz-Fas3G::3xFLAG*

517

518 Figure 4H, I (Top to Bottom, Left to Right)

519 *w/w or Y; Or42b-Gal4, Ubi-FRT-STOP-FRT-mCD8::DQVD::QF2/UASz-*

520 *3xFLAG::mNeonGreen; UAS-FLP, QUAS-tdTomato::3xHA/+*

521 *w/w or Y; Or42b-Gal4, Ubi-FRT-STOP-FRT-mCD8::DQVD::QF2/+; UAS-FLP, QUAS-*
522 *tdTomato::3xHA/UASz-Fas3G::3xFLAG*
523 *w/w or Y; Or42b-Gal4, Ubi-FRT-STOP-FRT-mCD8::DQVD::QF2/UAS-Diap-1::VENUS;*
524 *UAS-FLP, QUAS-tdTomato::3xHA/UASz-Fas3G::3xFLAG*
525
526 Figure 4–figure supplement 1C, D (Top to Bottom, Left to Right)
527 *w/w or Y; Or42b-Gal4, Ubi-FRT-STOP-FRT-mCD8::DQVD::QF2/UAS-LacZ-RNAi; UAS-*
528 *FLP, QUAS-tdTomato::3xHA/+*
529 *w/w or Y; Or42b-Gal4, Ubi-FRT-STOP-FRT-mCD8::DQVD::QF2/+; UAS-FLP, QUAS-*
530 *tdTomato::3xHA/UAS-Fas3-RNAi #1*
531 *w/w or Y; Or42b-Gal4, Ubi-FRT-STOP-FRT-mCD8::DQVD::QF2/+; UAS-FLP, QUAS-*
532 *tdTomato::3xHA/UAS-Fas3-RNAi #2*
533 *w/w or Y; Or42b-Gal4, Ubi-FRT-STOP-FRT-mCD8::DQVD::QF2/UAS-Fas3G-RNAi; UAS-*
534 *FLP, QUAS-tdTomato::3xHA/+*
535
536 Figure 4–figure supplement 1E (Left to Right, Top to Bottom)
537 *w, Pebbled-Gal4/Y; UASz-Drice::myc::mNeonGreen/+*
538 *w, Pebbled-Gal4/Y; UASz-Drice::myc::mNeonGreen/+; UASz-Fas3G::3xFLAG/+*
539 *w, Pebbled-Gal4/Y; UASz-Drice::myc::mNeonGreen/+; UAS-Fas3-RNAi #1/+*
540 *w, Pebbled-Gal4/Y; UASz-Drice::myc::mNeonGreen/+; UAS-Fas3-RNAi #2/+*
541 *w, Pebbled-Gal4/Y; UASz-Drice::myc::mNeonGreen/UAS-Fas3G-RNAi*
542
543 Figure 5A (Left to Right)
544 *w, Pebbled-Gal4/Y*
545 *w, Pebbled-Gal4/Y;; Dronc::V5::TurboID/+*

546 *w, Pebbled-Gal4/Y;; Dronc::V5::TurboID/UASz-Fas3G::3xFLAG*

547

548 Figure 5B (Left to Right)

549 *w, Pebbled-Gal4/Y;; Dronc::V5::TurboID/+*

550 *w, Pebbled-Gal4/Y;; Dronc::V5::TurboID/UASz-Fas3G::3xFLAG*

551 *w, Pebbled-Gal4/Y;; Dronc::V5::TurboID/UASz-Fas3C::3xFLAG*

552

553 Figure 5C, D (Top to Bottom, Left to Right)

554 *w/w or Y; Or42b-Gal4, Ubi-FRT-STOP-FRT-mCD8::DQVD::QF2/UASz-*

555 *3xFLAG::mNeonGreen; UAS-FLP, QUAS-tdTomato::3xHA/+*

556 *w/w or Y; Or42b-Gal4, Ubi-FRT-STOP-FRT-mCD8::DQVD::QF2/+; UAS-FLP, QUAS-*

557 *tdTomato::3xHA/UASz-Fas3G::3xFLAG*

558 *w/w or Y; Or42b-Gal4, Ubi-FRT-STOP-FRT-mCD8::DQVD::QF2/UAS-Dronc-RNAi; UAS-*

559 *FLP, QUAS-tdTomato::3xHA/UASz-Fas3G::3xFLAG*

560 *w/w or Y; Or42b-Gal4, Ubi-FRT-STOP-FRT-mCD8::DQVD::QF2/UAS-Dronc^{DN}; UAS-FLP,*

561 *QUAS-tdTomato::3xHA/UASz-Fas3G::3xFLAG*

562

563 Figure 5E (Left to Right)

564 *w, Pebbled-Gal4/Y;; Drice::V5::TurboID/+*

565 *w, Pebbled-Gal4/Y;; Drice::V5::TurboID/UASz-Fas3G::3xFLAG*

566 *w, Pebbled-Gal4/Y; +/UAS-Dronc-RNAi; Drice::V5::TurboID/UASz-Fas3G::3xFLAG*

567 *w, Pebbled-Gal4/Y; +/UAS-Dronc^{DN}; Drice::V5::TurboID/UASz-Fas3G::3xFLAG*

568

569 Figure 6B, C (Left to Right)

570 *w/Y; Or42b-Gal4/UASz-3xFLAG::mNeonGreen*

571 *w/Y; Or42b-Gal4/+; +/UASz-Fas3G::3xFLAG*

572 *w/Y; Or42b-Gal4/UAS-Dronc-RNAi; +/UASz-Fas3G::3xFLAG*

573 *w/Y; Or42b-Gal4/UAS-Dronc^{DN}; +/UASz-Fas3G::3xFLAG*

574

575 ***Protein preparation from Drosophila tissues***

576 Adult heads or brains of the given genotype were dissected in phosphate-buffered saline (PBS)
577 and lysed with RIPA buffer (50 mM Tris-HCl, pH 8.0, 150 mM Sodium Chloride, 0.5 w/v%
578 Sodium Deoxycholate, 0.1% w/v Sodium Dodecyl Sulfate, and 1.0% w/v NP-40) supplemented
579 with cOmplete ULTRA EDTA-free protease inhibitor cocktail (#05892953001, Roche).
580 Samples were homogenized and centrifuged at 20,000 ×g, 4°C for 10 min. The supernatants
581 were collected and snap-frozen in liquid nitrogen. Protein concentrations were determined
582 using the BCA assay (#297-73101, WAKO) following the manufacturer's protocol. The
583 samples were mixed with 6x Laemmli buffer, boiled at 95°C for 5 min, and then subjected to
584 purification of biotinylated proteins and western blot analysis.

585

586 ***Western blotting***

587 Each sample was separated using SDS-PAGE. The proteins were then transferred onto
588 Immobilon-P PVDF membranes (#IPVH00010; Millipore) for immunoblotting. Membranes
589 were blocked with 4% skim milk diluted in 1× TBST. Immunoblotting was performed using
590 the antibodies mentioned below diluted in 4% skim milk diluted in 1× TBST. Signals were
591 visualized using Immobilon Western Chemiluminescent HRP Substrate (#WBKLS0500;
592 Millipore) and FUSION SOLO. 7S. EDGE imaging station (Vilber-Lourmat). Contrast and
593 brightness adjustments were applied equally using Fiji (ImageJ) software (NIH Image).

594 The primary antibodies used included mouse anti-V5 monoclonal antibody (1:5,000,
595 #46-0705, Invitrogen), mouse anti-FLAG M2 monoclonal antibody (1:5,000, Sigma), mouse

596 anti-alpha tubulin (DM1A) monoclonal antibody (1:10,000, #T9026, Sigma), mouse anti-Actin
597 monoclonal antibody (1:5,000; #A4700, Sigma), mouse anti-Fasciclin 3 (7G10) antibody (1:50,
598 #AB_528238, DSHB), rabbit anti-Fasciclin3 isoform G antibody (1:50, this study), mouse anti-
599 Drosophila Lamin B monoclonal antibody (1:1000, #ADL67.10, DSHB). The secondary
600 antibodies used included goat anti-rabbit IgG HRP-conjugated antibody (1:5,000, #7074S,
601 CST) and goat/rabbit/donkey anti-mouse IgG HRP Conjugate (1:5,000, #W402B, Promega).
602 The membranes for streptavidin blotting were blocked with 3% BSA diluted in 1× TBST.
603 Streptavidin blotting was performed using streptavidin-horseradish peroxidase (1:10,000,
604 #SA10001; Invitrogen) diluted in 3% BSA diluted in 1× TBST.
605
606 ***Co-immunoprecipitation***
607 Adult heads were lysed on ice using DDM IP lysis buffer (50 mM Tris-HCl (pH 7.5), 150 mM
608 NaCl, 0.2% N-Dodecyl-β-D-maltoside (DDM) (#341-06161, WAKO)) containing cOmplete
609 ULTRA EDTA-free protease inhibitor cocktail. The samples were adjusted to 150 μg
610 protein/150 μL DDM IP lysis buffer. The samples were incubated overnight at 4 °C with 10
611 μL anti-FLAG M2 Magnetic Beads (#M8823-1ML, Millipore) equilibrated with the DDM IP
612 lysis buffer. The beads were washed three times in wash buffer (50 mM Tris-HCl (pH 7.5),
613 150 mM NaCl, 0.1% DDM) and boiled for 5 min at 95 °C with 50 μL 1× Laemmli buffer. The
614 samples were magnetically separated, and the supernatants were subjected to SDS-PAGE.
615
616 ***Immunohistochemistry***
617 Adult brains were dissected in PBS and fixed in 4% paraformaldehyde (PFA) at room
618 temperature for 30 min. Adult brains were washed three times with 0.3% PBST (Triton-X100)
619 for 10 min. After blocking with 5.0% normal donkey serum (#S30, Millipore)/PBST (PBSTn)
620 for 30 minutes at room temperature, tissues were incubated with primary antibody/PBSTn

621 overnight at 4°C. The samples were then washed with PBST three times for 10 min each and
622 incubated with secondary antibody/PBSTn for 2 h at room temperature. After incubation, the
623 tissues were washed with PBST three times for 10 min. Streptavidin and Hoechst 33342 were
624 added during secondary antibody incubation. The samples were mounted on glass slides with
625 SlowFade Gold antifade reagent (#S36939, Invitrogen). Images were captured using a Leica
626 TCS SP8 microscope (Leica Microsystems). Images were analyzed and edited using the Fiji
627 (ImageJ) software. For MASCaT analysis, newly eclosed adults were raised at 29°C for 1 week.
628 Classification of the MASCaT signal was performed by optically assessing the tdTomato
629 intensity. For cell number analysis, newly eclosed adults were raised at 29°C for 1 week. The
630 antennae were dissected as previously described (Karim et al., 2014), fixed with 4% PFA at
631 room temperature for 30 min, and washed with 0.4% PBST (Triton-X100) three times for 10
632 min. Quantification of cell numbers in antenna was performed using Fiji (ImageJ) software
633 using "3D object counter" for RedStinger positive cells.

634 The primary antibodies used were mouse anti-Fasciclin 3 (7G10) antibody (1:20,
635 #AB_528238, DSHB), rat anti-GFP (GF090R) monoclonal antibody (1:100, #04404-26,
636 nacalai Tesque), mouse anti-FLAG M2 monoclonal antibody (1:500, F1804, Sigma), and rat
637 anti-mCD8 monoclonal antibody (1:50, #MCD0800, Invitrogen). The secondary antibodies
638 used included Alexa Fluor 488-conjugated donkey anti-mouse IgG antibody (1:500, #A-21202,
639 ThermoFisher Scientific), Alexa Fluor 488-conjugated donkey anti-rat IgG antibody (1:500,
640 #A-21208, ThermoFisher Scientific), Alexa Fluor 647-conjugated donkey anti-mouse IgG
641 antibody (1:500, #A-31571, ThermoFisher Scientific), and Alexa Fluor 633-conjugated goat
642 anti-rat IgG antibody (1:500, #A-21094, ThermoFisher Scientific). The nuclei were stained
643 with Hoechst 33342 (8 μM, #H3570, Invitrogen). Streptavidin-Cy2 (1:500, #016-220-084,
644 Jackson ImmunoResearch) and Streptavidin-Cy5 (1:500, #016-170-084, Jackson
645 ImmunoResearch) were used to stain the biotinylated proteins.

646

647 ***Experimental design for LC-MS/MS analyses***

648 Two biological replicates were analyzed for each experimental condition to determine the
649 relative abundance of *Drice::V5::TurboID/w*^{1118}.

650

651 ***Purification of biotinylated proteins***

652 Samples were prepared as previously described (Shinoda et al., 2023). Briefly, 100 μg of
653 biotinylated protein-containing lysate (from 100 brains or 20 heads) was subjected to FG-
654 NeutrAvidin bead (#TAS8848 N1171, Tamagawa Seiki) purification. The FG-NeutrAvidin
655 beads (25 μL, approximately 500 μg) were washed three times with RIPA buffer. Benzonase-
656 treated biotinylated protein samples suspended in 1 mL RIPA buffer were incubated overnight
657 at 4°C. Conjugated beads were magnetically isolated and washed with 500 μL of an ice-cold
658 RIPA buffer solution, 1 M KCl solution, 0.1 M Na_2CO_3 solution and 4 M urea solution. For
659 western blot analyses, the purified samples were mixed with Laemmli buffer, boiled at 95°C
660 for 5 min, and then subjected to western blot analysis. For LC-MS/MS analysis, the purified
661 samples were washed with 500 μL ultrapure water (#214-01301, WAKO) and 500 μL of 50
662 mM ammonium bicarbonate (AMBC). The samples were then mixed with 50 μL of 0.1%
663 Rapigest diluted in 50 mM AMBC, and 5 μL of 50 mM TCEP was subsequently added.
664 Samples were incubated at 60°C for 5 min, and then 2.5 μL 200 mM MMTS was added. One
665 microgram sequence-grade modified trypsin (#V5111, Promega) was then added for on-bead
666 trypsin digestion at 37°C for 16 h. The beads were magnetically isolated and 60 μL of the
667 supernatant was collected. Then, 3 μL 10% TFA was added to the supernatants, and the samples
668 were incubated at 37°C for 60 min with gentle agitation. The samples were then centrifuged at
669 20,000 ×g, 4°C for 10 min. The peptides were desalinated and purified using a GL-tip SDB
670 (#7820-11200, GL Sciences) following the manufacturer's protocol. The samples were speed-

671 backed at 45°C for 30 min and dissolved in 25 µL of 0.1% formic acid. The samples were then
672 centrifuged at 20,000 ×g, 4°C for 10 min, and the supernatants were collected. The peptide
673 concentrations were determined using the BCA assay. Finally, 500 ng of the purified protein
674 was subjected to LC-MS/MS analysis.
675
676 ***LC-MS/MS analyses***
677 LC-MS/MS analyses were performed as previously described (Shinoda et al., 2023). Briefly,
678 samples were loaded onto Acclaim PepMap 100 C18 column (75 µm x 2 cm, 3 µm particle size
679 and 100 Å pore size; #164946, ThermoFisher Scientific) and separated on nano-capillary C18
680 column, (75 µm x 12.5 cm, 3 µm particle size, #NTCC-360/75-3-125, Nikkyo Technos) using
681 EASY-nLC 1200 system (ThermoFisher Scientific). The elution conditions are listed in Table
682 S3. The separated peptides were analyzed using QExactive (ThermoFisher Scientific) in data-
683 dependent MS/MS mode. The parameters for the MS/MS analysis are listed in Table S4. The
684 collected data were analyzed using Proteome Discoverer (PD) 2.2 software with the Sequest
685 HT search engine. The parameters for the PD 2.2 analysis are described in Table S5. Peptides
686 were filtered at a false discovery rate of 0.01 using the Percolator node. Label-free
687 quantification was performed based on the intensities of the precursor ions using a precursor-
688 ion quantifier node. Normalization was performed using the total amount of peptides in all
689 average scaling modes. Proteins with 10 folds or higher abundance relative to the control (w^{1118})
690 were considered for further analysis. MS proteomic data were deposited in the
691 ProteomeXchange Consortium via the jPOST partner repository with the dataset identifier
692 PXD042922 (Okuda et al., 2017).
693
694 ***Gene Ontology analysis***

695 Gene Ontology (GO) analysis of cellular components was performed using DAVID (Huang et
696 al., 2009).
697
698 ***Generation of rabbit polyclonal anti-Fasciclin 3 isoform G antibody***
699 The peptide corresponding to the 506–524 AA (N-LKPANEATPATTPAPTTAA-C) of Fas3G
700 was used by Eurofins Inc. to immunize rabbits to raise a polyclonal antibody. The antibody was
701 affinity purified using the same peptide provided by Eurofins, Inc.
702
703 ***IDR prediction***
704 Amino acid sequences were obtained from the FlyBase database [https://flybase.org/].
705 Disordered intracellular regions of Fas3 isoforms were predicted using the PSIPRED protein
706 sequence analysis workbench in DISOPRED3 [http://bioinf.cs.ucl.ac.uk/psipred/].
707
708 ***Protein complexes prediction with AlphaFold2-Multimer***
709 Amino acid sequences were obtained from the FlyBase database [https://flybase.org/]. Protein
710 complexes were predicted using ColabFold v1.5.5: AlphaFold2 using MMseqs2 (Mirdita et al.,
711 2022) with the following settings: template_mode:none, msa_mode: mmseqs2_uniref_env,
712 pair_mode: unpaired_paired, model_type: alphafold2_multimer_v3, num_recycles: 3. PAE
713 plots of the structural models ranked first among five models were selected as representatives.
714
715 ***Molecular cloning***
716 For all isoforms (A, B/F, C, D/E, G) of *pUASz-Fasciclin 3::3xFLAG*, the coding sequences of
717 Fasciclin 3s were PCR-amplified using 3xFLAG-tag harboring primers from *Drosophila* cDNA
718 and were ligated into the *BamH*I/*Kpn*I-digested *pUASz1.0* vector (#1431, *Drosophila* Genomics
719 Resource Center (DGRC)) (DeLuca and Spradling, 2018) using In-Fusion (#Z9648N,

720 TaKaRa). For all isoforms of *pAc5-Fasciclin 3::3xFLAG*, the coding sequence of *Fasciclin*
721 *3s::3xFLAG* were PCR-amplified from corresponding *pUASz-Fasciclin 3::3xFLAG* vectors
722 and were ligated into the *Eco*RI/*Xho*I-digested *pAc5-STABLE2-neo* vector (#32426, Addgene)
723 (González et al., 2011) using NEBuilder HiFi DNA Assembly (#E2621L, NEB). For *pUASz-*
724 *3xFLAG::mNeonGreen*, the coding sequence of mNeonGreen was PCR-amplified using
725 3xFLAG-tag harboring primers from *pAc5-V5::mNeonGreen* (Shinoda et al., 2023) and ligated
726 into the *Xho*I-digested *pUASz1.0* vector using In-Fusion. For *pUASz-*
727 *Drice::myc::mNeonGreen*, the coding sequence of mNeonGreen was PCR-amplified from
728 *pAc5-V5::mNeonGreen* using myc-tag-harboring primers. The coding sequence of Drice was
729 PCR-amplified from *Drosophila* cDNA. The two fragments were then ligated into the *Xho*I-
730 digested *pUASz1.0* vector using In-Fusion. For *pUASz-V5::TurboID* and *pUASz-*
731 *Caspase::V5::TurboID*, the coding sequences of *Dcp-1*, *Drice* and *Dronc* were PCR amplified
732 from *Drosophila* cDNA. The coding sequence of V5::TurboID was PCR-amplified from *V5-*
733 *TurboID-NES_pcDNA3* (#107169; Addgene). The two fragments were then ligated into the
734 *Xho*I-digested *pUASz1.0* vector using In-Fusion. Catalytic dead mutations (Dcp-1: C196G
735 (TGC to GGC), Drice: C211G (TGC to GGC), and Dronc: C318G (TGC to GGC)) were
736 introduced by PCR-based site-directed mutagenesis, and the corresponding fragments were
737 ligated into the *Xho*I-digested *pUASz1.0* vector using In-Fusion. For *pJFRC-*
738 *mCD8::DQVD/A::QF2*, the coding sequence of *mCD8::DQVD/A* were PCR-amplified from
739 genomic DNA of *Caspase-Sensitive/Insensitive-Gal4* (Tang et al., 2015). The coding sequence
740 of *QF2* was PCR-amplified from *pBPQU* vector (Kashio et al., 2016). These fragments were
741 ligated into the *Xho*I/*Xba*I-digested *pJFRC-28K* vector (a gift from H. Kazama) using In-
742 Fusion. For *pUbi-FRT-STOP-FRT-mCD8::DQVD/A::QF2*, the FRT-STOP-FRT cassette
743 sequence was PCR amplified from *pJFRC201-10xUAS-FRT-STOP-FRT-myr::smGFP-HA*
744 (#63166; Addgene). The coding sequence of mCD8::DQVD/A was PCR-amplified from the

745 genomic DNA of *Caspase-Sensitive/Insensitive-Gal4* (Tang et al., 2015). The coding sequence
746 of QF2 was PCR amplified from the *pBPQUw* plasmid (Kashio et al., 2016). The three
747 fragments were ligated into *EcoR*I-digested *pUbi83* vector (a gift from D. Umetsu) using In-
748 Fusion. For *pQUAST-mNeonGreen*, the coding sequence of mNeonGreen was PCR-amplified
749 from *pAc5-V5::mNeonGreen* and ligated into the *EcoR*I-digested *pQUAST* (#24349, Addgene)
750 vector using In-Fusion. For *pUASz-FLPo*, the coding sequences of FLPo were PCR-amplified
751 from *pQUAST-FLPo* (#24357, Addgene) and ligated into the *Xho*I-digested *pUASz1.0* vector
752 using In-Fusion. For *pWALIUM20-Fas3G-shRNA*, the top and bottom oligonucleotides
753 including *mRNA* sequence specific to isoform G (5'-AATGAACCAAAGCAAGACAAA-3')
754 were annealed in annealing buffer (10 mM Tris-HCl, 0.1 M NaCl, 1 mM EDTA). The annealed
755 fragment was ligated into *Nhe*I/*Eco*RI-digested *pWALIUM20* (#1472, DGRC) vector using
756 DNA Ligation Kit <Mighty Mix> (#6023, TaKaRa).

757 All established plasmids were sequenced by Eurofins, Inc. The detailed plasmid DNA
758 sequences are available upon request. The established plasmids were injected into y^1, w^{67c23};
759 *P[CaryP]attP40* (*pUASz-3xFLAG::mNeonGreen*, *pUASz-Drice::myc::mNeonGreen*, *pUbi-*
760 *FRT-STOP-FRT-mCD8::DQVD/A::QF2* and *pWALIUM20-Fas3G-shRNA*) or y^1, w^{67c23};
761 *P[CaryP]attP2* (*pUASz-Fasciclin 3s::3xFLAG*, *pUASz-V5::TurboID* and *pUASz-*
762 *Caspase::V5::TurboID*) for PhiC31-mediated transgenesis (BestGene Inc.). Each red-eye-
763 positive transformant was isogenized. Integration of the attP landing site was confirmed using
764 genomic PCR.

765

766 ***Cell culture***

767 *Drosophila* S2 cells were grown at 25°C in Schneider's *Drosophila* medium (#21720001,
768 GIBCO) supplemented with 10% (v/v) heat-inactivated fetal bovine serum, 100 U/ml penicillin,
769 and 100 μg/ml streptomycin (#168-23191, WAKO). Cells were seeded in 24-well plates and

770 transfected with the desired plasmids using Effectene Transfection Reagent (#301427,
771 QIAGEN) following the manufacturer's protocol. Sixteen hours after transfection, the cells
772 were reseeded into CELL CULTURE DISH, PS, 35/10 MM (#627870, Grainer BIO-ONE) and
773 incubated for 24 h. Images were obtained using a Leica AF6000 DMI6000 B microscope (Leica
774 Microsystems). Images were analyzed and edited using Fiji software (NIH Image).

775 For the substrate cleavage assay, cells were seeded in 12-well plates and were
776 transfected with desired *pAc5-Fas3::3xFLAG* plasmids using Effectene Transfection Reagent
777 following the manufacturer's protocol. After 40 h of incubation, the cells were treated with 10
778 μg/mL cycloheximide (CHX, #C7698, Sigma) for apoptosis induction. After 6 h of incubation,
779 cells were collected using RIPA buffer supplemented with cOmplete ULTRA EDTA-free
780 protease inhibitor cocktail depending on the cell status. For apoptotic cell lysate collection, cells
781 were resuspended by pipetting and were collected into a 1.5 mL tube. The cells were then
782 centrifuged at 800 ×g, 4 °C for 5 min, resuspended in PBS, and centrifuged again using the same
783 parameters. The cell pellets were then lysed with 100 μL RIPA buffer. For the other
784 experimental conditions, the cells were washed thrice with PBS and directly lysed on the plate
785 with 100 μL RIPA buffer. The supernatants were collected and snap-frozen in liquid nitrogen.
786 Protein concentrations were determined using the BCA assay following the manufacturer's
787 protocol. The samples were mixed with 6x Laemmli buffer, boiled at 95°C for 5 min, and then
788 subjected to western blot analysis.

789 For the validation of Fas3G-shRNA, cells were seeded in 12-well plates and were co-
790 transfected with *pActin-Gal4,* desired *pUASz-Fas3::3xFLAG* and *pWALIUM20-empty* or
791 *pWALIUM20-Fas3G-shRNA* plasmids using Effectene Transfection Reagent following the
792 manufacturer's protocol. After 40 h of incubation, the cells were washed thrice with PBS and
793 directly lysed on the plate with 100 μL RIPA buffer. The supernatants were collected and snap-
794 frozen in liquid nitrogen. Protein concentrations were determined using the BCA assay

795 following the manufacturer's protocol. The samples were mixed with 6x Laemmli buffer,
796 boiled at 95°C for 5 min, and then subjected to western blot analysis.
797
798 ***Aging experiment***
799 Adult male flies were raised in vials containing 15 fly/vial, and incubated at 29°C, 65%
800 humidity with 12h/12h light/dark cycle. The flies were transferred every 2–4 days to vials
801 containing fresh food.
802
803 ***Two choice preference assay***
804 Newly eclosed adult male flies were raised in vials containing 25 fly/vial, and incubated at 29°C,
805 65% humidity with 12h/12h light/dark cycle. The flies were transferred every 2–4 days to vials
806 containing fresh food for 1 week. The flies were starved in MilliQ (MQ) for 4 h prior to the
807 assay. About 75 flies were put in 1000-mL glass beaker, which contained two standards bottles
808 filled with 500 µl 1% ACV (Mizkan) and 500 µl MQ. The bottles were then covered with
809 sponge plugs containing pipette tips. The pipette tip was cut to increase the size of the opening
810 such that only one fly could climb into the bottle at a time. The glass beaker was covered with
811 a mesh fabric. The beakers were set in an incubator at 29°C for 2 hr for the assay. The
812 experiments were evaluated only if at least one of the tested flies entered either of 2 bottles.
813 The preference index equaled the number of flies in the ACV minus the number of flies in the
814 MQ, divided by the number of total live flies in both inside and outside of the bottles, and
815 multiplied by 100. Values greater than zero indicate a preference for 1% ACV and values less
816 than zero indicate aversion. We repeated the same experiment with different sets of flies and
817 the number of times is indicated by N.
818
819 ***Statistical analysis***

820 Statistical analyses were performed using the GraphPad Prism 8 software (MDF). Data are
821 shown as the means ± standard error of the mean. *P*-values were calculated using a one-way
822 analysis of variance (ANOVA) with Bonferroni correction (Figure 4B for selected pairs, Figure
823 4D for every pair). *P*-values were calculated using the chi-square test with Bonferroni's
824 correction, with mNeonGreen as a control (Figure 4G), LacZ-RNAi as a control (Figure 4–
825 figure supplement 1D), mNeonGreen and Fas3G as controls (Figure 4I, 5D), and mNeonGreen
826 as a control (Figure 6C). *P*-values were calculated using one-way ANOVA with Dunnett's
827 multiple comparison test (Figure 6B, mNeonGreen as a control). NS: $P > 0.05$, †: < 0.05.
828

829 **Acknowledgments**

830 We would like to thank Dr. D. Umetsu, Dr. H. Kazama, Addgene and *Drosophila* Genomics
831 Resource Center for providing plasmids, Dr. Y. Nitta, Dr. A. Sugie, and Dr. T. Ichinose for
832 helpful discussions, and the Bloomington *Drosophila* Stock Center, Vienna Drosophila
833 Resource Center and Kyoto Stock Center for providing the fly strains. We thank Dr. S.
834 Hirayama, Dr. S. Murata, and the one-stop sharing faculty center for future drug discovery at
835 the Graduate School of Pharmaceutical Sciences, University of Tokyo, for the LC-MS/MS
836 analysis. We thank Miura's lab members for their technical assistance and discussions; in
837 particular, K. Takenaga for preparing the fly food, and R. Takamoto for experimental support.
838 The MASCaT was established by MASaya Muramoto with critical advice from members of
839 Shu MASuda at MASayuki Miura Laboratories. We would like to thank *Editage*
840 (www.editage.com) for English language editing of this manuscript. This work was supported
841 by grants from the Ministry of Education, Culture, Sports, Science, and Technology of Japan
842 (KAKENHI Grant Numbers 19K16137, 21K15080, 22H05586, and 23K05747 to N.S. and
843 21H04774, 21K19206 and 23H04766 to M.Mi.), the Japan Agency for Medical Research and
844 Development (AMED; Grant number JP21gm5010001 to M.Mi.), and grants from the Takeda
845 Science Foundation and Sumitomo Foundation to N.S.

846

847 **Author Contributions**

848 M.Mi. and N.S. designed the study; M.Mu., N.H. and N.S. conducted all the experiments and
849 analyzed all the data; M.O. and T.C. supervised the two choice preference assay; M.Mu., N.H.,
850 M.Mi. and N.S. wrote the manuscript.

851

852 **Conflict of Interests**

853 The authors declare that they have no conflict of interest.

854 **References**

855 Amcheslavsky A, Wang S, Fogarty CE, Lindblad JL, Fan Y, Bergmann A. 2018. Plasma
856 membrane localization of apoptotic caspases for non-apoptotic functions. *Dev Cell*
857 **45**:450-464.e3.
858 Aram L, Yacobi-Sharon K, Arama E. 2017. CDPs: caspase-dependent non-lethal cellular
859 processes. *Cell Death Differ* **24**:1307–1310.
860 Boucher D, Blais V, Denault J-B. 2012. Caspase-7 uses an exosite to promote poly(ADP ribose)
861 polymerase 1 proteolysis. *Proc Natl Acad Sci U S A* **109**:5669–5674.
862 Branon TC, Bosch JA, Sanchez AD, Udeshi ND, Svinkina T, Carr SA, Feldman JL, Perrimon
863 N, Ting AY. 2018. Efficient proximity labeling in living cells and organisms with
864 TurboID. *Nat Biotechnol* **36**:880–887.
865 Campbell DS, Okamoto H. 2013. Local caspase activation interacts with Slit-Robo signaling to
866 restrict axonal arborization. *J Cell Biol* **203**:657–672.
867 Cheriyamkunnel SJ, Rose S, Jacob PF, Blackburn LA, Glasgow S, Moorse J, Winstanley M,
868 Moynihan PJ, Waddell S, Rezaval C. 2021. A neuronal mechanism controlling the
869 choice between feeding and sexual behaviors in Drosophila. *Curr Biol* **31**:4231-4245.e4.
870 Chiba A, Snow P, Keshishian H, Hotta Y. 1995. Fasciclin III as a synaptic target recognition
871 molecule in Drosophila. *Nature* **374**:166–168.
872 Chihara T, Kitabayashi A, Morimoto M, Takeuchi K-I, Masuyama K, Tonoki A, Davis RL,
873 Wang JW, Miura M. 2014. Caspase inhibition in select olfactory neurons restores innate
874 attraction behavior in aged Drosophila. *PLoS Genet* **10**:e1004437.
875 D'Brot A, Chen P, Vaishnav M, Yuan S, Akey CW, Abrams JM. 2013. Tango7 directs cellular
876 remodeling by the Drosophila apoptosome. *Genes Dev* **27**:1650–1655.
877 Dehkordi MH, Munn RGK, Fearnhead HO. 2022. Non-canonical roles of apoptotic caspases in
878 the nervous system. *Front Cell Dev Biol* **10**:840023.
879 DeLuca SZ, Spradling AC. 2018. Efficient expression of genes in the Drosophila germline
880 using a UAS promoter free of interference by Hsp70 piRNAs. *Genetics* **209**:381–387.
881 Desroches A, Denault J-B. 2019. Caspase-7 uses RNA to enhance proteolysis of poly(ADP-
882 ribose) polymerase 1 and other RNA-binding proteins. *Proc Natl Acad Sci U S A*
883 **116**:21521–21528.
884 Ding AX, Sun G, Argaw YG, Wong JO, Easwaran S, Montell DJ. 2016. CasExpress reveals
885 widespread and diverse patterns of cell survival of caspase-3 activation during
886 development in vivo. *Elife* **5**. doi:10.7554/eLife.10936
887 Ditzel M, Broemer M, Tenev T, Bolduc C, Lee TV, Rigbolt KTG, Elliott R, Zvelebil M,
888 Blagoev B, Bergmann A, Meier P. 2008. Inactivation of effector caspases through
889 nondegradative polyubiquitylation. *Mol Cell* **32**:540–553.
890 Dorstyn L, Colussi PA, Quinn LM, Richardson H, Kumar S. 1999. DRONC, an ecdysone-
891 inducible Drosophila caspase. *Proc Natl Acad Sci U S A* **96**:4307–4312.
892 Evans R, O'Neill M, Pritzel A, Antropova N, Senior A, Green T, Žídek A, Bates R, Blackwell
893 S, Yim J, Ronneberger O, Bodenstein S, Zielinski M, Bridgland A, Potapenko A, Cowie
894 A, Tunyasuvunakool K, Jain R, Clancy E, Kohli P, Jumper J, Hassabis D. 2021. Protein
895 complex prediction with AlphaFold-Multimer. *bioRxiv*.
896 doi:10.1101/2021.10.04.463034
897 González M, Martín-Ruíz I, Jiménez S, Pirone L, Barrio R, Sutherland JD. 2011. Generation
898 of stable Drosophila cell lines using multicistronic vectors. *Sci Rep* **1**:75.
899 Green DR. 2019. The coming decade of cell death research: Five riddles. *Cell* **177**:1094–1107.
900 Gu Q, Jiao S, Duan K, Wang Y-X, Petralia RS, Li Z. 2021. The BAD-BAX-caspase-3 cascade
901 modulates synaptic vesicle pools via autophagy. *J Neurosci* **41**:1174–1190.
902 Hay BA, Wassarman DA, Rubin GM. 1995. Drosophila homologs of baculovirus inhibitor of

903 apoptosis proteins function to block cell death. *Cell* **83**:1253–1262.
904 Huang DW, Sherman BT, Lempicki RA. 2009. Bioinformatics enrichment tools: paths toward
905 the comprehensive functional analysis of large gene lists. *Nucleic Acids Res* **37**:1–13.
906 Igaki T, Kanda H, Yamamoto-Goto Y, Kanuka H, Kuranaga E, Aigaki T, Miura M. 2002. Eiger,
907 a TNF superfamily ligand that triggers the Drosophila JNK pathway. *EMBO J* **21**:3009–
908 3018.
909 Julien O, Wells JA. 2017. Caspases and their substrates. *Cell Death Differ* **24**:1380–1389.
910 Kang Y, Neuman SD, Bashirullah A. 2017. Tango7 regulates cortical activity of caspases
911 during reaper-triggered changes in tissue elasticity. *Nat Commun* **8**:603.
912 Kanuka H, Kuranaga E, Takemoto K, Hiratou T, Okano H, Miura M. 2005. Drosophila caspase
913 transduces Shaggy/GSK-3beta kinase activity in neural precursor development. *EMBO*
914 *J* **24**:3793–3806.
915 Karim MR, Endo K, Moore AW, Taniguchi H. 2014. Whole mount immunolabeling of
916 olfactory receptor neurons in the Drosophila antenna. *J Vis Exp*. doi:10.3791/51245-v
917 Kashio S, Obata F, Zhang L, Katsuyama T, Chihara T, Miura M. 2016. Tissue nonautonomous
918 effects of fat body methionine metabolism on imaginal disc repair in Drosophila. *Proc*
919 *Natl Acad Sci U S A* **113**:1835–1840.
920 Kose H, Rose D, Zhu X, Chiba A. 1997. Homophilic synaptic target recognition mediated by
921 immunoglobulin-like cell adhesion molecule Fasciclin III. *Development* **124**:4143–
922 4152.
923 Koto A, Kuranaga E, Miura M. 2009. Temporal regulation of Drosophila IAP1 determines
924 caspase functions in sensory organ development. *J Cell Biol* **187**:219–231.
925 Kumar S. 2007. Caspase function in programmed cell death. *Cell Death Differ* **14**:32–43.
926 Kumar S, Dorstyn L, Lim Y. 2022. The role of caspases as executioners of apoptosis. *Biochem*
927 *Soc Trans* **50**:33–45.
928 Lee TV, Fan Y, Wang S, Srivastava M, Broemer M, Meier P, Bergmann A. 2011. Drosophila
929 IAP1-mediated ubiquitylation controls activation of the initiator caspase DRONC
930 independent of protein degradation. *PLoS Genet* **7**:e1002261.
931 Li L, Ding Z, Pang T-L, Zhang B, Li C-H, Liang A-M, Wang Y-R, Zhou Y, Fan Y-J, Xu Y-Z.
932 2020. Defective minor spliceosomes induce SMA-associated phenotypes through
933 sensitive intron-containing neural genes in Drosophila. *Nat Commun* **11**:5608.
934 Li Z, Jo J, Jia J-M, Lo S-C, Whitcomb DJ, Jiao S, Cho K, Sheng M. 2010. Caspase-3 activation
935 via mitochondria is required for long-term depression and AMPA receptor
936 internalization. *Cell* **141**:859–871.
937 Luck K, Kim D-K, Lambourne L, Spirohn K, Begg BE, Bian W, Brignall R, Cafarelli T,
938 Campos-Laborie FJ, Charloteaux B, Choi D, Coté AG, Daley M, Deimling S,
939 Desbuleux A, Dricot A, Gebbia M, Hardy MF, Kishore N, Knapp JJ, Kovács IA,
940 Lemmens I, Mee MW, Mellor JC, Pollis C, Pons C, Richardson AD, Schlabach S,
941 Teeking B, Yadav A, Babor M, Balcha D, Basha O, Bowman-Colin C, Chin S-F, Choi
942 SG, Colabella C, Coppin G, D'Amata C, De Ridder D, De Rouck S, Duran-Frigola M,
943 Ennajdaoui H, Goebels F, Goehring L, Gopal A, Haddad G, Hatchi E, Helmy M, Jacob
944 Y, Kassa Y, Landini S, Li R, van Lieshout N, MacWilliams A, Markey D, Paulson JN,
945 Rangarajan S, Rasla J, Rayhan A, Rolland T, San-Miguel A, Shen Y, Sheykhkarimli D,
946 Sheynkman GM, Simonovsky E, Taşan M, Tejeda A, Tropepe V, Twizere J-C, Wang
947 Y, Weatheritt RJ, Weile J, Xia Y, Yang X, Yeger-Lotem E, Zhong Q, Aloy P, Bader
948 GD, De Las Rivas J, Gaudet S, Hao T, Rak J, Tavernier J, Hill DE, Vidal M, Roth FP,
949 Calderwood MA. 2020. A reference map of the human binary protein interactome.
950 *Nature* **580**:402–408.
951 Mirdita M, Schütze K, Moriwaki Y, Heo L, Ovchinnikov S, Steinegger M. 2022. ColabFold:
952 making protein folding accessible to all. *Nat Methods* **19**:679–682.

953 Mukherjee A, Williams DW. 2017. More alive than dead: non-apoptotic roles for caspases in
954 neuronal development, plasticity and disease. *Cell Death Differ* **24**:1411–1421.
955 Nakajima Y-I, Kuranaga E. 2017. Caspase-dependent non-apoptotic processes in development.
956 *Cell Death Differ* **24**:1422–1430.
957 Ohsawa S, Hamada S, Kuida K, Yoshida H, Igaki T, Miura M. 2010. Maturation of the olfactory
958 sensory neurons by Apaf-1/caspase-9-mediated caspase activity. *Proc Natl Acad Sci U*
959 *S A* **107**:13366–13371.
960 Okuda S, Watanabe Y, Moriya Y, Kawano S, Yamamoto T, Matsumoto M, Takami T,
961 Kobayashi D, Araki N, Yoshizawa AC, Tabata T, Sugiyama N, Goto S, Ishihama Y.
962 2017. jPOSTrepo: an international standard data repository for proteomes. *Nucleic*
963 *Acids Res* **45**:D1107–D1111.
964 Orme MH, Liccardi G, Moderau N, Feltham R, Wicky-John S, Tenev T, Aram L, Wilson R,
965 Bianchi K, Morris O, Monteiro Domingues C, Robertson D, Tare M, Wepf A, Williams
966 D, Bergmann A, Gstaiger M, Arama E, Ribeiro PS, Meier P. 2016. The unconventional
967 myosin CRINKLED and its mammalian orthologue MYO7A regulate caspases in their
968 signalling roles. *Nat Commun* **7**:10972.
969 Qin W, Cho KF, Cavanagh PE, Ting AY. 2021. Deciphering molecular interactions by
970 proximity labeling. *Nat Methods* **18**:133–143.
971 Semmelhack JL, Wang JW. 2009. Select Drosophila glomeruli mediate innate olfactory
972 attraction and aversion. *Nature* **459**:218–223.
973 Shinoda N, Hanawa N, Chihara T, Koto A, Miura M. 2019. Dronc-independent basal
974 executioner caspase activity sustains Drosophila imaginal tissue growth. *Proc Natl Acad*
975 *Sci U S A* **116**:20539–20544.
976 Shinoda N, Horikoshi M, Taira Y, Muramoto M, Hirayama S, Murata S, Miura M. 2023.
977 Caspase cleaves Drosophila BubR1 to modulate spindle assembly checkpoint function
978 and lifespan of the organism. *FEBS J* **290**:4200–4223.
979 Takemoto K, Nagai T, Miyawaki A, Miura M. 2003. Spatio-temporal activation of caspase
980 revealed by indicator that is insensitive to environmental effects. *J Cell Biol* **160**:235–
981 243.
982 Tang HL, Tang HM, Fung MC, Hardwick JM. 2015. In vivo CaspaseTracker biosensor system
983 for detecting anastasis and non-apoptotic caspase activity. *Sci Rep* **5**:9015.
984 Valente P, Lignani G, Medrihan L, Bosco F, Contestabile A, Lippiello P, Ferrea E, Schachner
985 M, Benfenati F, Giovedì S, Baldelli P. 2016. Cell adhesion molecule L1 contributes to
986 neuronal excitability regulating the function of voltage-gated Na+ channels. *J Cell Sci*
987 **129**:1878–1891.
988 Verghese S, Bedi S, Kango-Singh M. 2012. Hippo signalling controls Dronc activity to regulate
989 organ size in Drosophila. *Cell Death Differ* **19**:1664–1676.
990 Walsh JG, Cullen SP, Sheridan C, Lüthi AU, Gerner C, Martin SJ. 2008. Executioner caspase-
991 3 and caspase-7 are functionally distinct proteases. *Proc Natl Acad Sci U S A*
992 **105**:12815–12819.
993 Westphal D, Sytnyk V, Schachner M, Leshchyns'ka I. 2010. Clustering of the neural cell
994 adhesion molecule (NCAM) at the neuronal cell surface induces caspase-8- and -3-
995 dependent changes of the spectrin meshwork required for NCAM-mediated neurite
996 outgrowth. *J Biol Chem* **285**:42046–42057.
997 Williams DW, Kondo S, Krzyzanowska A, Hiromi Y, Truman JW. 2006. Local caspase activity
998 directs engulfment of dendrites during pruning. *Nat Neurosci* **9**:1234–1236.
999

1000 **Figures & Figure Legends**

1001 **Figure 1**

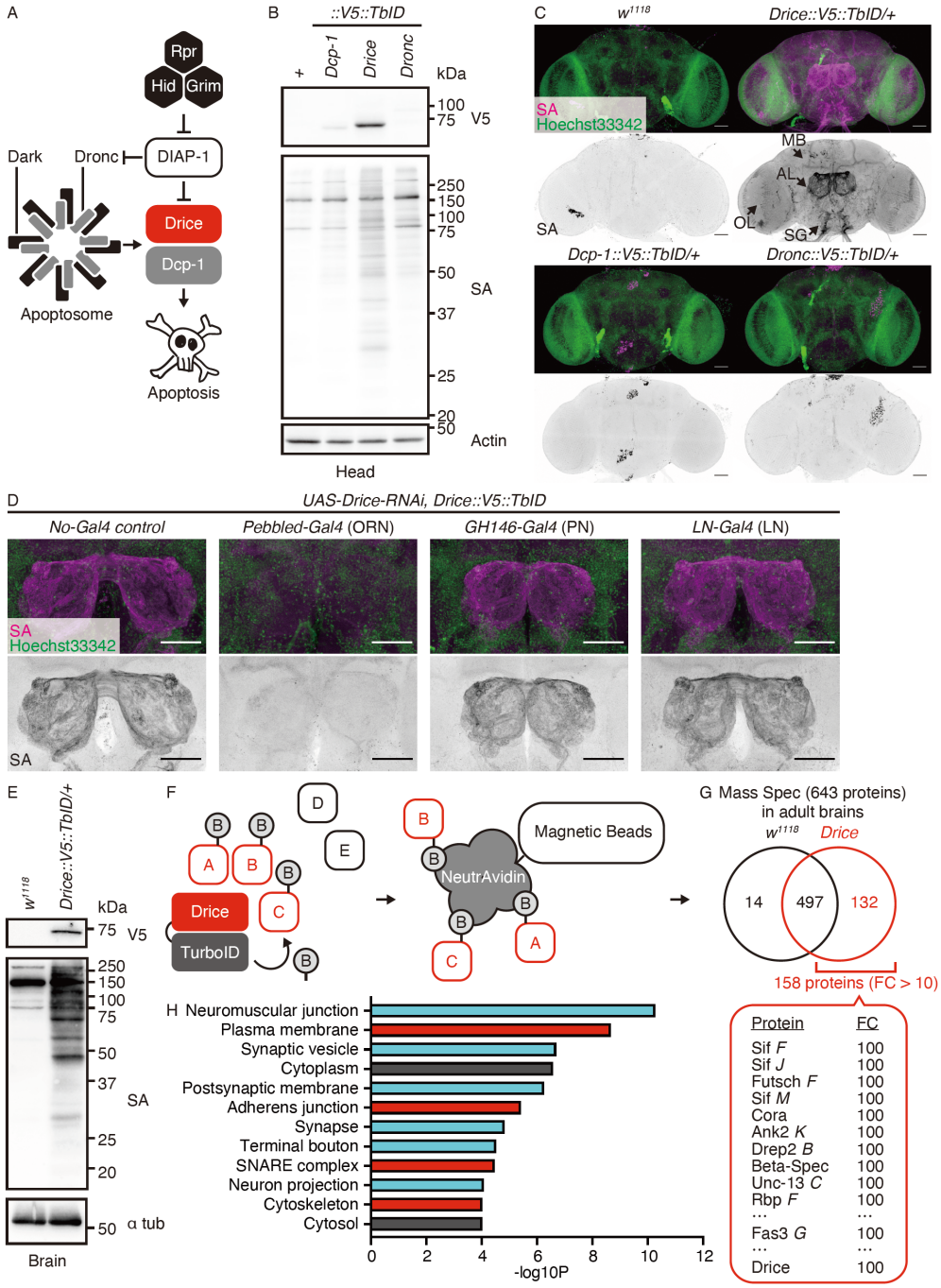

1002

1003 **Figure 1. Expression patterns and proximal proteins of Drice in the adult brain.**

1004 (A) Schematic diagram of *Drosophila* apoptosis signaling.

1005 (B) Western blot of expression of caspases in adult male heads.

1006 (C) Representative images of adult male brains. Expression patterns of each caspase are

1007 visualized using Streptavidin (SA, magenta). Nuclei are visualized by Hoechst33342 (Green).

1008 Scale bar: 50 μm.

1009 (D) Representative images of antennal lobes (ALs) in the adult female brains. Expression
1010 patterns of Drice are visualized using SA (magenta). Nuclei are visualized by Hoechst33342
1011 (Green). Scale bar: 50 µm.
1012 (E) Western blot of proteins extracted from adult male brains.
1013 (F) Schematic diagram of the TurboID-mediated identification of proximal proteins.
1014 (G) A summary of mass spectrometry analysis of proteins of the adult male brains. Partial list
1015 of Drice proximal proteins and their Fold Change (FC) are shown.
1016 (H) Gene Ontology analysis (Cellular Compartment) of 158 Drice proximal proteins
1017 (*Drice::V5::TurboID*/w^{1118} > 10). Cyan: neuronal-related fraction, Red: membrane fraction.
1018

1019 **Figure 1–figure supplement 1**

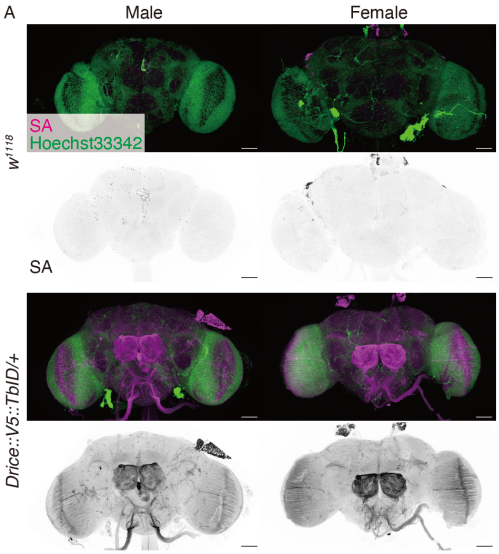

1020

1021 **Figure 1–figure supplement 1. Expression patterns of Drice in the adult brain in males**
1022 **and females.**

1023 (A) Representative images of adult male and female brains. Expression patterns of Drice are
1024 visualized using Streptavidin (SA, magenta). Nuclei are visualized by Hoechst33342 (Green).
1025 Scale bar: 50 µm.

1026

1027 **Figure 2**

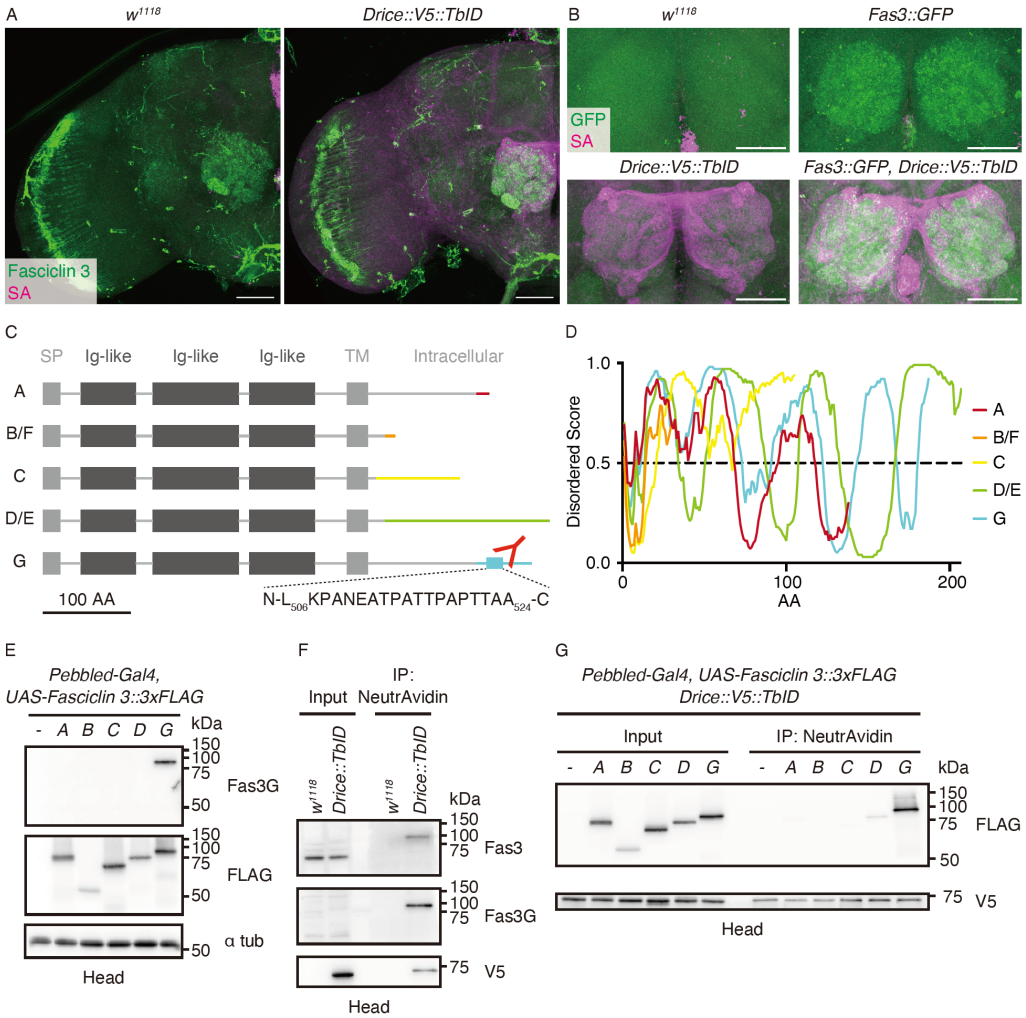

1028

1029 **Figure 2. A specific isoform of Fasciclin 3 is in proximity to Drice.**

1030 (A) Representative expression patterns of Drice (Streptavidin (SA); magenta) and Fasciclin 3
1031 (Fas3, anti-Fasciclin 3 antibody staining; green) in the adult male brains. Scale bar: 50 μm.
1032 (B) Representative expression patterns of Drice (SA; magenta) and Fas3 (anti-GFP antibody
1033 staining; green) in the antennal lobes (ALs) of the adult male brains. Scale bar: 50 μm.
1034 (C) Schematic protein structures of Fas3 isoforms. Intracellular regions differ from each other.
1035 A peptide region used to raise anti-Fas3G antibody is shown.
1036 (D) IDR predictions of intracellular regions of each protein isoform.
1037 (E) Western blot of proteins extracted from adult heads. Anti-Fas3G antibody specifically
1038 detects Fas3 isoform G.
1039 (F) Western blot of adult male heads. Drice proximal proteins were purified using NeturAvidin.
1040 (G) Western blot of adult head proteins. Drice proximal proteins were purified using
1041 NeturAvidin.
1042

1043 **Figure 2–figure supplement 1**

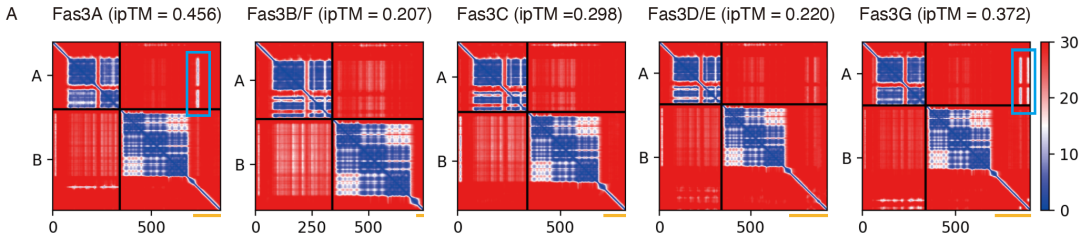

1044

1045 **Figure 2–figure supplement 1. Predicted protein complexes of Drice and each Fas3**
1046 **isoform**

1047 (A) Predicted aligned error (PAE) plots of protein complex of Drice and each Fas3 isoform
1048 generated by AlphaFold2-Multimer. A represents Drice and B represents each Fas3 isoform.
1049 Numbers in X axis represent amino acid position. The intracellular region of each Fas3 isoform
1050 is represented by the orange bar. Potential interaction sites predicted by low PAE scores in
1051 Drice-Fas3A/G are highlighted by blue rectangles.

1052

1053 **Figure 2–figure supplement 2**

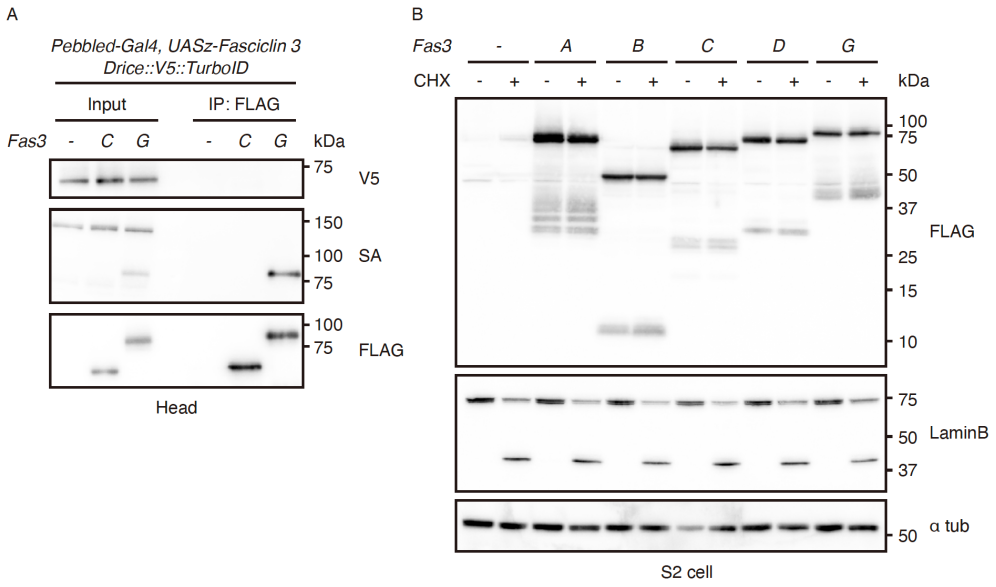

1054

1055 **Figure 2–figure supplement 2. Biochemical property of Fas3s with caspases.**

1056 (A) Co-immunoprecipitation of 3xFLAG-tagged Fas3s with V5-tagged Drice extracted from

1057 adult male heads.

1058 (B) Western blot for 3xFLAG-tagged Fas3s expressed in *Drosophila* S2 cells. Apoptosis was

1059 induced by treating S2 cells with cycloheximide (CHX).

1060

1061 **Figure 3**

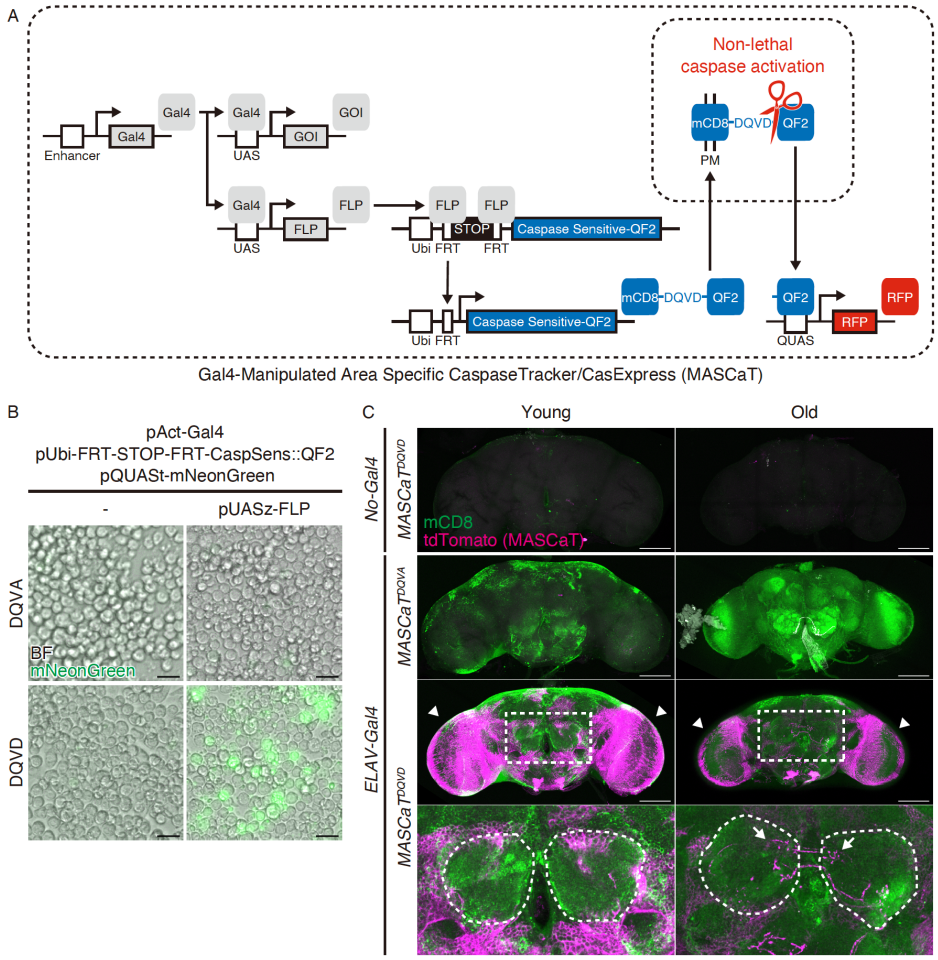

1062

1063 **Figure 3. A Gal4-Manipulated Area Specific CaspaseTracker/CasExpress (MASCaT).**

1064 (A) A schematic diagram of MASCaT expressed using the Gal4/UAS system with FLP-
1065 mediated recombination. Caspase sensitive-QF2 is activated by caspase-mediated cleavage at
1066 the plasma membrane.

1067 (B) Representative images of S2 cells expressing caspase sensitive-QF2 probes by the
1068 Gal4/UAS system with FLP-mediated recombination. Scale bar: 20 µm.

1069 (C) Representative images of adult male brains of young (1 week old) and old (3 weeks old)
1070 flies raised at 29°C. Arrowheads indicate optic lobes. Magnified images (white rectangle) show
1071 antennal lobes (ALs; white circles). Arrows indicate age-dependent caspase activation at the
1072 ALs. Scale bar: 100 µm.

1073

1074 **Figure 3–figure supplement 1**

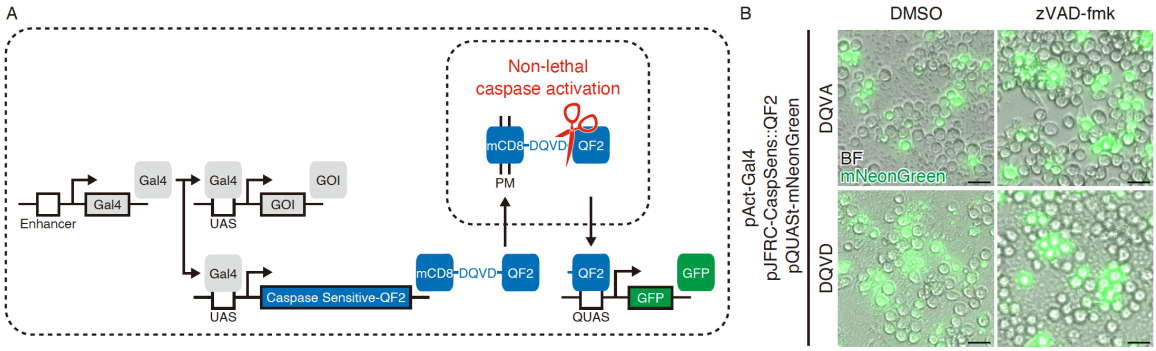

1075

1076 **Figure 3–figure supplement 1. Overexpression of *mCD8::DQVD::QF2* probes in**
1077 ***Drosophila* S2 cells.**

1078 (A) A schematic diagram of MASCaT expressed directly using the Gal4/UAS system. Caspase
1079 sensitive-QF2 is activated by caspase-mediated cleavage at the plasma membrane.

1080 (B) Representative images of S2 cells expressing caspase sensitive-QF2 probes directly by the
1081 Gal4/UAS system. A pan-caspase inhibitior, zVAD-fmk, is treated to inhibit caspase activity.
1082 Scale bar: 20 μm.

1083

1084 **Figure 4**

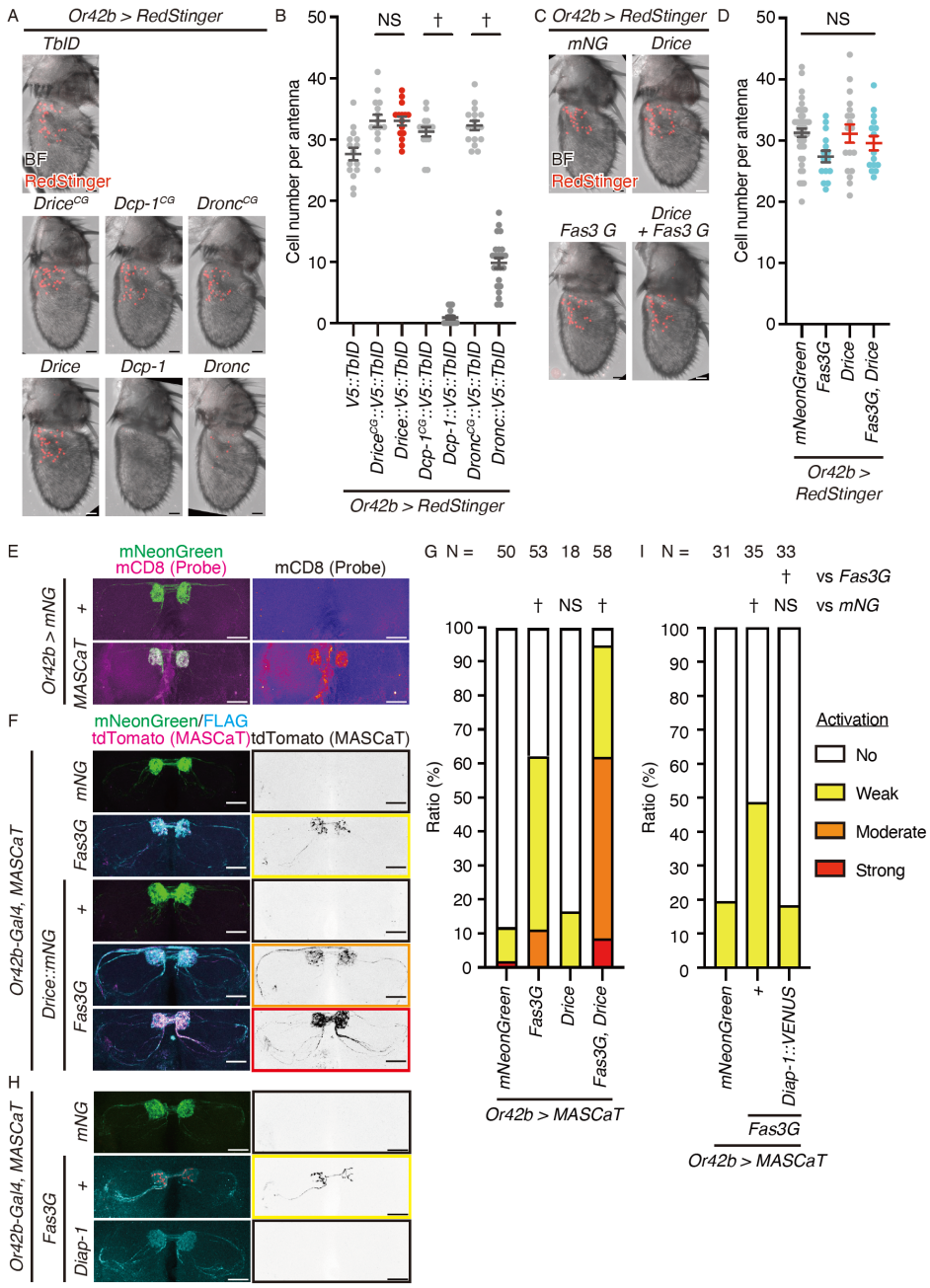

1085

1086 **Figure 4. *Fasciclin 3 isoform G* overexpression enhances non-lethal caspase activation.**

1087 (A) Representative images of the adult male antennae of 1 weeks old flies raised at 29°C. Cell

1088 bodies are visualized using RedStinger (red). Scale bar: 20 µm.

1089 (B) Quantification of cell number of (A). Data are presented as mean ± SEM. *P*-values were

1090 calculated using one-way analysis of variance (ANOVA) with Bonferroni's correction for

1091 selected pairs. NS: $P > 0.05$, †: $P < 0.05$. Sample sizes: V5::TbID (N = 15), Drice^{CG}::V5::TbID

1092 (N = 15), Drice::V5::TbID (N = 15), Dcp-1^{CG}::V5::TbID (N = 15), Dcp-1::V5::TbID (N = 16),

1093 Dronc^{CG}:::V5::TbID (N = 16), Dronc:::V5::TbID (N = 23).

1094 (C) Representative images of the adult male antennae of 1 week old flies raised at 29°C. Cell
1095 bodies are visualized using RedStinger (red). Scale bar: 20 μm.
1096 (D) Quantification of cell number of (C). Data are presented as mean ± SEM. *P*-values were
1097 calculated using one-way ANOVA with Bonferroni's correction for every pair. NS: $P > 0.05$,
1098 †: $P < 0.05$. Sample sizes: mNeonGreen (N = 44), Fas3G (N = 15), Drice (N = 18), Fas3G +
1099 Drice (N = 15).
1100 (E) Representative images of the antennal lobes (ALs) of male brains of 1 week old flies raised
1101 at 29°C expressing MASCaT probe (mCD8, magenta). Scale bar: 30 μm.
1102 (F) Representative images of the ALs of brains of 1 week old flies raised at 29°C with caspase
1103 activation visualized by MASCaT. Scale bar: 30 μm.
1104 (G) Quantifications of caspase activity detected by MASCaT of (F). *P*-values were calculated
1105 using chi-square test with Bonferroni's correction using mNeonGreen as control. NS: $P > 0.05$,
1106 †: $P < 0.05$. Sample sizes are shown in the graph.
1107 (H) Representative images of the ALs of brains of 1 week old flies raised at 29°C with caspase
1108 activation visualized by MASCaT. Scale bar: 30 μm.
1109 (I) Quantifications of caspase activity detected by MASCaT of (H). *P*-values were calculated
1110 using chi-square test with Bonferroni's correction using mNeonGreen and Fas3G as controls,
1111 respectively. NS: $P > 0.05$, †: $P < 0.05$. Sample sizes are shown in the graph.
1112

1113 **Figure 4–figure supplement 1**

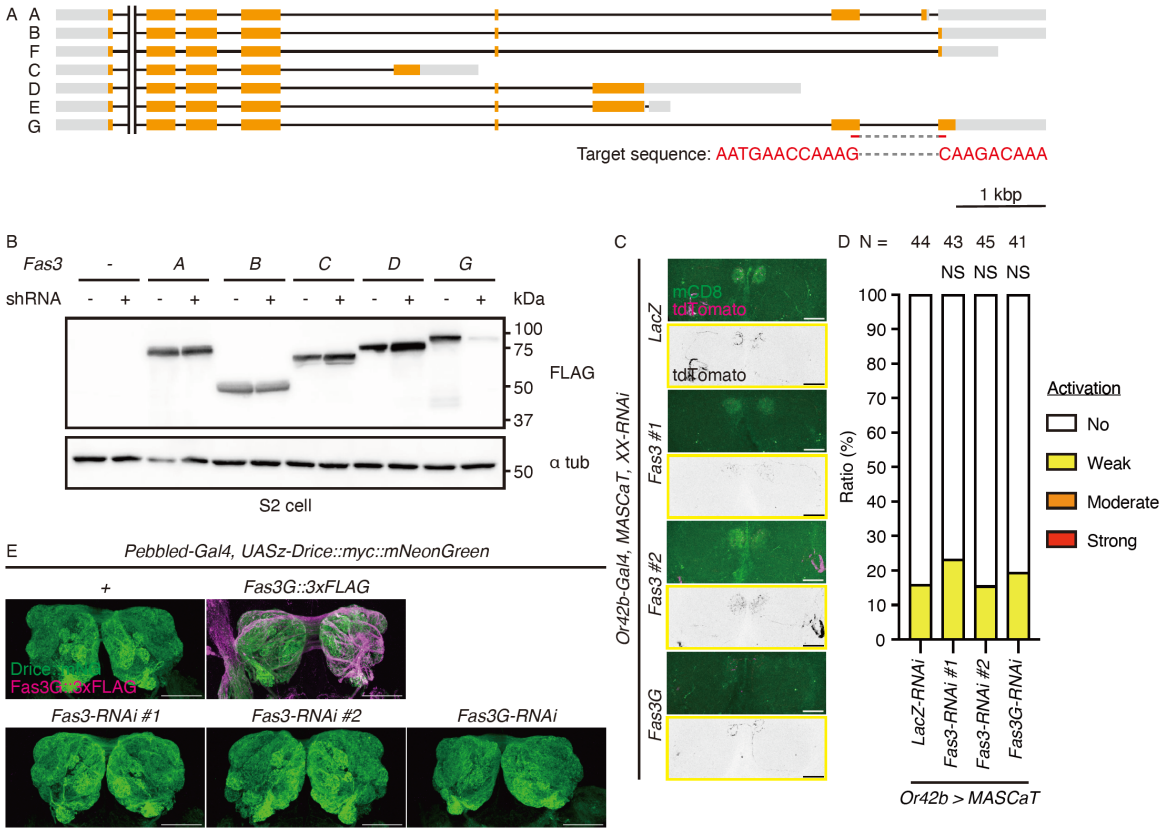

1114

1115 **Figure 4–figure supplement 1. Loss of function analysis of Fas3G.**

1116 (A) Gene structure of Fas3. CDS (orange) and UTR (grey) are shown in boxes. Target sequence

1117 of Fas3G-shRNA is shown in red.

1118 (B) Western blot for 3xFLAG-tagged Fas3s expressed in S2 cells with Fas3G-shRNA.

1119 (C) Representative images of the ALs of brains of 1 week old flies raised at 29°C with caspase

1120 activation visualized by MASCaT. Scale bar: 30 µm.

1121 (D) Quantifications of caspase activity detected by MASCaT of (C). *P*-values were calculated

1122 using chi-square test with Bonferroni's correction using *LacZ-RNAi* as control. NS: $P > 0.05$.

1123 Sample sizes are shown in the graph.

1124 (E) Representative images of the ALs of brains of 1 week old flies expressing mNeonGreen-

1125 tagged Drice (green) and 3xFLAG-tagged Fas3G (magenta). Scale bar: 50 µm.

1126

1127 **Figure 5**

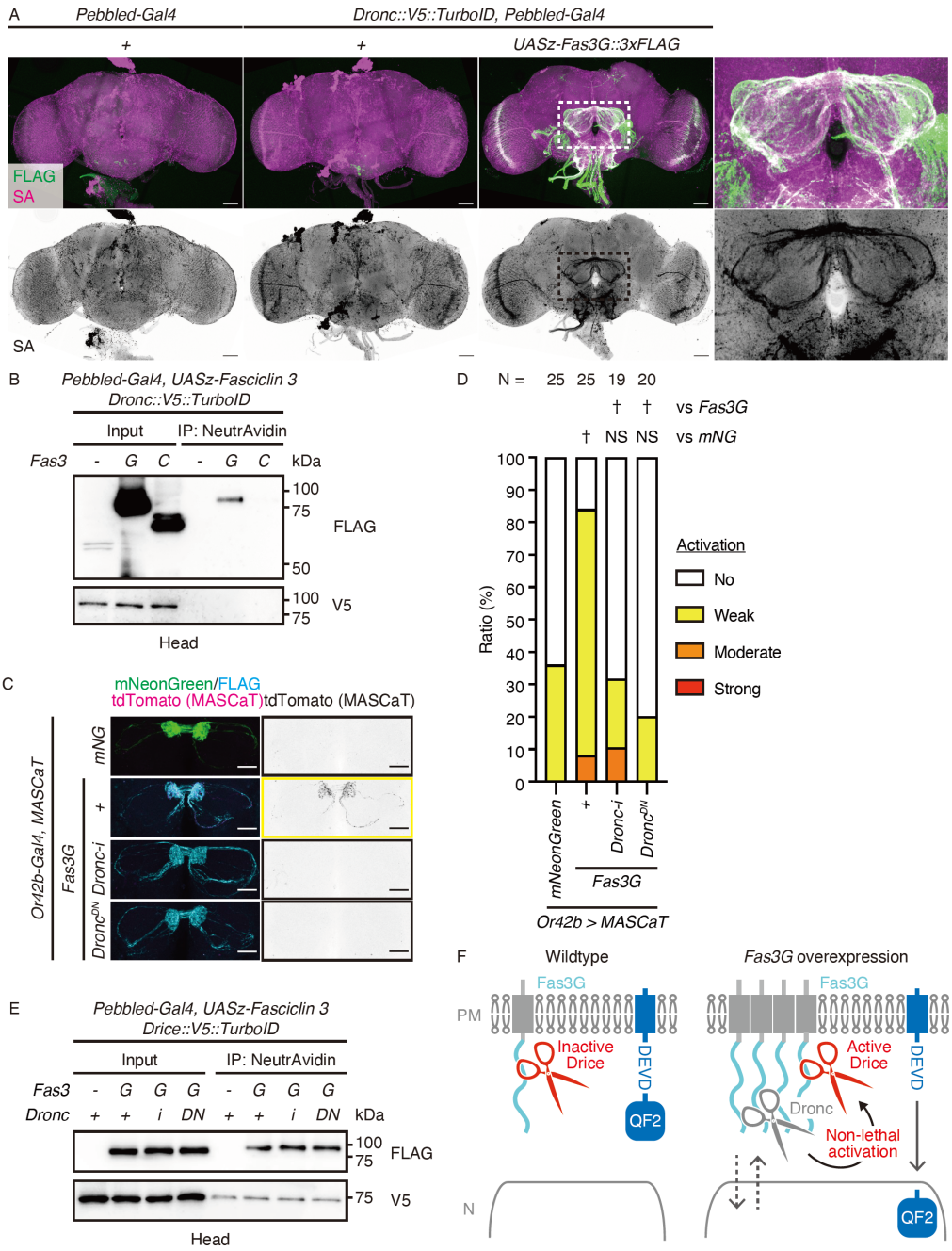

1128

1129 **Figure 5. *Fasciclin 3 isoform G* overexpression enhances non-lethal caspase activation in**
1130 **a Dronc-dependent manner.**

1131 (A) Representative images of adult male brains. Expression patterns of Dronc are visualized
1132 using Streptavidin (SA, magenta). Magnified images (white rectangle) show antennal lobes
1133 (ALs). Scale bar: 50 µm.

1134 (B) Western blot of adult male heads. Dronc proximal proteins were purified using NeturAvidin.

1135 (C) Representative images of the AL of brains of 1 week old flies raised at 29°C with caspase
1136 activation visualized using MASCaT. Scale bar: 30 µm.

1137 (D) Quantifications of caspase activity detected using MASCaT of (C). *P*-values were
1138 calculated using chi-square test with Bonferroni's correction using mNeonGreen and Fas3G as
1139 controls, respectively. NS: $P > 0.05$, †: $P < 0.05$. Sample sizes are shown in the graph.
1140 (E) Western blot of adult male heads. Drice proximal proteins were purified using NeturAvidin.
1141 (F) A schematic model of subcellularly restricted non-lethal caspase activation upon Fas3G
1142 overexpression.
1143

1144 **Figure 6**

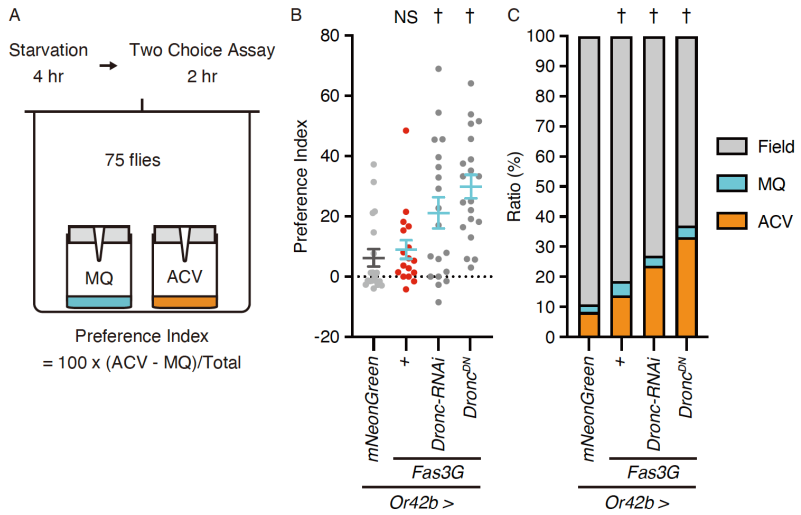

1145

1146 **Figure 6. *Fasciclin 3 isoform G* overexpression-facilitated caspase activation regulates**
1147 **attraction behavior.**

1148 (A) Schematic diagram of two choice preference assay. Flies are starved for 4 hours before the
1149 assay. Flies are left for 2 hours in the bottle. Preference index is calculated by counting the
1150 number of flies left in MQ, ACV and other (field) compartments.

1151 (B) Preference index of 1 week old male flies raised at 29°C in response to 1% apple cider
1152 vinegar in two choice preference assay. Data are presented as mean ± SEM. *P*-values were
1153 calculated using one-way ANOVA followed by Dunnets' multiple comparison test using
1154 mNeonGreen as a control. NS: $P > 0.05$, †: $P < 0.05$. Sample sizes: mNG (N = 19 (1327 flies)),
1155 Fas3G (N = 17 (1191 flies)), Fas3G + Dronc-RNAi (N = 19 (1295 flies)), Fas3G + Dronc^{DN} (N
1156 = 20 (1320 flies)).

1157 (C) The ratio of flies in the given conditions in the two choice preference assay of (B). *P*-values
1158 were calculated using chi-square test with Bonferroni's correction using mNeonGreen as
1159 control. †: $P < 0.05$. Sample sizes: mNG (N = 1327 flies), Fas3G (N = 1191 flies), Fas3G +
1160 Dronc-RNAi (N = 1295 flies), Fas3G + Dronc^{DN} (N = 1320 flies).

1161

1162 **Legends for Table S1–5**

1163 **Table S1. Proximal protein list.** A list of the identified proximal proteins (Abundance ratio
1164 (Drice::V5::TurboID/Control) > 10). The UniProt Accessions, Gene Description, and
1165 Abundance Ratio (Drice::V5::TurboID/Control) are listed.

1166

1167 **Table S2. Gene Ontology analysis.** The result of Gene Ontology (GO) analysis of Cellular
1168 Compartment for Drice proximal proteins. GO term, P values, Fold Enrichment, Count and
1169 Genes are listed.

1170

1171 **Table S3. LC settings.** Gradient settings for LC analysis are presented.

1172

1173 **Table S4. MS/MS settings.** Settings used for the MS/MS analysis are presented.

1174

1175 **Table S5. Proteome Discoverer 2.2 settings.** Proteome Discoverer 2.2 settings for proteomics
1176 analysis are presented.

1177